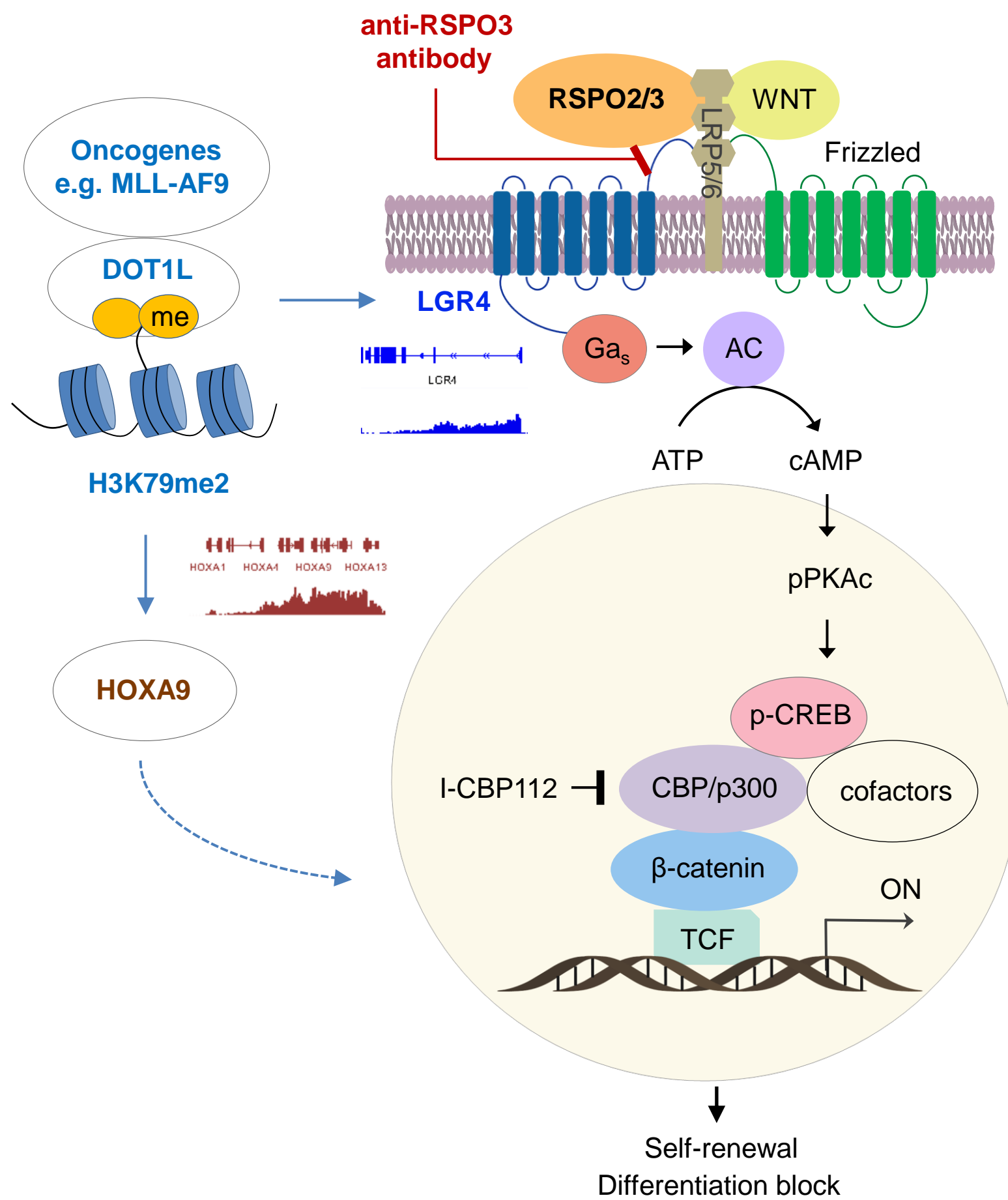


Cancer Cell

Targeting RSPO3-LGR4 signaling for leukemia stem cell eradication in acute myeloid leukemia

--Manuscript Draft--

Manuscript Number:	CANCER-CELL-D-19-00234R4
Full Title:	Targeting RSPO3-LGR4 signaling for leukemia stem cell eradication in acute myeloid leukemia
Article Type:	Research Article
Keywords:	AML; Acute Myeloid Leukemia; signaling pathway; WNT/b-catenin; RSPO ligand; RSPO3; R-spondin; LGR4; HOXA9; LSCs; LSC; leukemia stem cells; self-renewal; differentiation; antibody-based therapy; anti-RSPO3 antibody; targeted therapy; PDX; patient-derived xenograft; preclinical testing; MLL-AF9; MLL fusion; MLL-rearranged AML; 9p deletion; patient specimens; preclinical models; therapeutic targeting; AML therapy; treatment; leukemia
Corresponding Author:	Jenny Y. Wang, Ph.D. University of New South Wales Randwick, AUSTRALIA
First Author:	Basit Salik
Order of Authors:	Basit Salik Hangyu Yi, Ph.D. Nunki Hassan Nancy Santiappillai Binje Vick, Ph.D. Patrick Connerty, Ph.D. Alastair Duly, Ph.D. Toby Trahair, MD Andrew Woo, Ph.D. Dominik Beck, Ph.D. Tao Liu, Ph.D. Karsten Spiekermann Irmela Jeremias, Ph.D. Jianlong Wang, Ph.D. Maria Kavallaris, Ph.D. Michelle Haber, Ph.D. Murray D Norris, Ph.D. Dan A Liebermann, Ph.D. Richard J D'Andrea, Ph.D. Christopher Murriel, Ph.D. Jenny Y. Wang, Ph.D.
Abstract:	Signals driving aberrant self-renewal in the heterogeneous leukemia stem cell (LSC) pool determine aggressiveness of acute myeloid leukemia (AML). We report that a positive modulator of canonical WNT signaling pathway, RSPO-LGR4, upregulates key self-renewal genes and is essential for LSC self-renewal in a subset of AML. RSPO2/3 serve as stem cell growth factors to block differentiation and promote proliferation of primary AML patient blasts. RSPO receptor, LGR4, is epigenetically upregulated and



Targeting RSPO3-LGR4 signaling for leukemia stem cell eradication in acute myeloid leukemia

AUTHORS: Basit Salik,^{1†} Hangyu Yi,^{1†} Nunki Hassan,^{1†} Nancy Santiappillai,¹ Binje Vick,^{2,3,4} Patrick Connerty,¹ Alastair Duly,¹ Toby Trahair,⁵ Andrew J. Woo,⁶ Dominik Beck,^{7,8} Tao Liu,⁵ Karsten Spiekermann,^{2,3,9} Irmela Jeremias,^{3,4,10} Jianlong Wang,¹¹ Maria Kavallaris,^{5,12} Michelle Haber,⁵ Murray D. Norris,⁵ Dan A. Liebermann,¹³ Richard J. D'Andrea,¹⁴ Christopher Murriel,¹⁵ and Jenny Y. Wang^{1,16*}

AFFILIATIONS

¹Cancer and Stem Cell Biology Group, Children's Cancer Institute, Lowy Cancer Research Centre, University of New South Wales, Sydney, NSW 2052, Australia

²German Cancer Research Center (DKFZ), Heidelberg, Germany

³German Cancer Consortium (DKTK), partner site Munich, Germany

⁴Research Unit Apoptosis in Hematopoietic Stem Cells, Helmholtz Zentrum München, German Research Center for Environmental Health, Munich, Germany

⁵Children's Cancer Institute, Lowy Cancer Research Centre, University of New South Wales, Sydney, NSW 2052, Australia

⁶Harry Perkins Institute of Medical Research, QEII Medical Centre, Nedlands and Centre for Medical Research, The University of Western Australia, Crawley, WA 6009, Australia

⁷Centre for Health Technologies and the School of Biomedical Engineering, University of Technology Sydney, Sydney, Australia

⁸Lowy Cancer Research Centre and the Prince of Wales Clinical School, University of New South Wales, Australia, Sydney, Australia

⁹Experimental Leukemia and Lymphoma Research (ELLF) Department of Internal Medicine 3, University Hospital, Ludwig-Maximilians-Universität München (LMU), Munich, Germany

¹⁰Department of Pediatrics, Dr. von Hauner Childrens Hospital, Ludwig Maximilians University, Munich, Germany

¹¹Department of Medicine, Columbia Center for Human Development, Columbia University Irving Medical Center, New York, NY 10032, USA

¹²Australian Centre for NanoMedicine and ARC Centre of Excellence in Convergent Bio-Nano-Science and Technology, University of New South Wales, Sydney, NSW 2052, Australia

¹³Fels Institute for Cancer Research and Molecular biology and Department of Medical Genetics & Molecular Biochemistry, School of Medicine, Temple University, Philadelphia, PA 19140, USA

¹⁴Acute Leukaemia Laboratory, Centre for Cancer Biology, University of South Australia and SA Pathology, Adelaide, South Australia, Australia

¹⁵OncoMed Pharmaceuticals, Inc. Redwood City, CA 94063, USA

¹⁶Lead Contact

†These authors contributed equally.

*Correspondence: jwang@ccia.unsw.edu.au (J.Y.W)

SUMMARY

Signals driving aberrant self-renewal in the heterogeneous leukemia stem cell (LSC) pool determine aggressiveness of acute myeloid leukemia (AML). We report that a positive modulator of canonical WNT signaling pathway, RSPO-LGR4, upregulates key self-renewal genes and is essential for LSC self-renewal in a subset of AML. RSPO2/3 serve as stem cell growth factors to block differentiation and promote proliferation of primary AML patient blasts. RSPO receptor, LGR4, is epigenetically upregulated and works through cooperation with HOXA9, a poor prognostic predictor. Blocking the RSPO3-LGR4 interaction by clinical-grade anti-RSPO3 antibody (OMP-131R10/rosmantuzumab) impairs self-renewal and induces differentiation in AML patient-derived xenografts but does not affect normal hematopoietic stem cells, providing a therapeutic opportunity for HOXA9-dependent leukemia.

SIGNIFICANCE

A fundamental challenge in the treatment of aggressive AML is relapse caused by the persistence of chemoresistant LSCs. Ablating LSCs by targeting deregulated self-renewal pathways is critical for successful anticancer therapy. Despite the recognized clinical importance, identification of pharmacologically tractable pathways required for self-renewal in a heterogeneous LSC pool remains largely unexplored. Here we uncover an essential role for a positive modulator of canonical WNT signaling, RSPO-LGR4, in promoting aberrant self-renewal in a subset of AML. RSPO3-LGR4 pathway could be effectively blocked by an anti-RSPO3 antibody (previously used in clinical trials for solid tumors) that abrogates leukemia-initiating capacity of patient-derived LSCs without harming the healthy stem cell compartment, thus providing a therapeutic window to specifically target LSCs.

INTRODUCTION

Self-renewal and differentiation block are two characteristic features of leukemia stem cells (LSCs) contributing to tumor heterogeneity and malignancy in acute myeloid leukemia (AML). Like the normal hematopoietic stem cell (HSC) compartment, LSCs derived from HSCs or committed progenitors are functionally heterogeneous in primary human AML, with varying degrees of self-renewal capacity and developmental potential (Hope et al., 2004). A high relapse rate in AML suggests that current standard intensive chemotherapy does not target quiescent and highly self-renewing LSCs and therefore only provides durable therapy for a minority of patients. Identifying signals critical for driving high self-renewal activity in a heterogeneous LSC pool, which determines disease aggressiveness, is still a largely unexplored research area essential for designing effective cancer therapies.

HOXA9 is a key regulator of normal and malignant stem cells and controls the self-renewal/differentiation switch (Abramovich and Humphries, 2005). High expression of HOXA9 is an indicator of poor survival in a broad range of malignancies and is observed in approximately 50% of AML patient samples with diverse cytogenetic abnormalities including translocations (Golub et al., 1999). Translocations involving the mixed-lineage leukemia (*MLL*) gene on chromosome 11q23, a relatively common cytogenetic abnormality in acute leukemia, result in the formation of chimeric MLL fusions (e.g., MLL-AF9) that are associated with poor outcome (Krivtsov and Armstrong, 2007; Muntean and Hess, 2012). In syngeneic mouse models, MLL-AF9 induces leukemic transformation of HSCs or committed progenitors by triggering an aberrant HOX-associated self-renewal gene expression program, including HOXA9 and the HOX cofactor MEIS1 (Krivtsov et al., 2006). HOXA9 and MEIS1 cooperate to block myeloid differentiation pathways prior to inducing AML in mice (Calvo et al., 2001; Kawagoe et al., 1999; Kroon et al., 1998; Lawrence et al., 1999). We and others have previously demonstrated that WNT/ β -catenin signaling is required for self-renewal of LSCs in murine models of AML induced by MLL fusion-transduced bone marrow (BM)/committed progenitors or by co-expression of key MLL fusion targets *HOXA9* and *MEIS1* in HSCs (Wang et al., 2010; Yeung et al., 2010). However, key molecules involved in driving constitutive activation of β -catenin signaling and their capacity to control LSC functions still

remain largely unclear.

WNT/ β -catenin signaling is often active in human cancers including AML (Clevers and Nusse, 2012; Simon et al., 2005; Ysebaert et al., 2006). Of note, while aberrant activation of β -catenin frequently occurs in human LSCs (Majeti et al., 2009; Yeung et al., 2010) and is associated with poor overall survival in AML patients (Ysebaert et al., 2006), increased expression of WNT proteins has not been observed. Conversely, in normal HSCs, WNT3 treatment activates β -catenin and results in increased proliferation *in vitro* and enhanced self-renewal *in vivo* of adult HSCs (Reya et al., 2003; Willert et al., 2003), whilst WNT3 deletion in fetal liver hematopoiesis leads to decreased HSC numbers and impaired long-term repopulating capacity of HSCs upon serial transplantation in mice (Luis et al., 2009). This suggests that aberrant activation of WNT/ β -catenin signaling in AML may require other developmental signaling molecules that function as agonists. The R-spondin ligands are candidates for such a role as they bind to and function through LGR4/LGR5 (leucine-rich repeat-containing G protein-coupled receptors) and synergize with low levels of WNT ligands to potentiate β -catenin activation in normal adult stem cells from several organs, such as the intestine (Carmon et al., 2011; Lynch and Wang, 2016). While the LGR proteins appear to be physically associated with the WNT receptor complex Frizzled-LRP5/6, the potency of R-spondins in enhancing WNT signals is not affected by the level of WNT receptors, but instead largely depends on the abundance of LGR expression (Carmon et al., 2011; de Lau et al., 2011). Notably, LGR4 is expressed predominantly in fetal liver long-term reconstituting HSCs (LT-HSCs) that have extensive self-renewal capacity, implicating a role for LGR4 in early hematopoietic development (Liu et al., 2014). Among R-spondin ligands (RSPO1-RSPO4), RSPO3 is prominently expressed in hematopoietic organs (Kazanskaya et al., 2008). These observations suggest a possible involvement of RSPO-LGR4 signaling in malignant hematopoiesis.

RESULTS

Inhibition of LGR4 exerts origin-specific blockade of aberrant self-renewal and AML progression

Consistent with previous observations, our integrated analysis of five independent microarray datasets (GSE13159, GSE15434, GSE61804, GSE14468 and The Cancer Genome Atlas TCGA) showed increased levels of *LGR4* but no noticeable changes of the related family member *LGR5* across 481 AML patient samples harboring diverse cytogenetic abnormalities including 11q23/MLL, compared with normal human HSCs (GSE42519, $p < 0.0291$; **Figure S1A**) (Bagger et al., 2016). LGR4 plays an essential role during development as genetic ablation of *Lgr4* in mice results in embryonic and perinatal lethality (Mazerbourg et al., 2004). To understand the functional involvement of LGR4 in leukemogenesis, we employed a lentiviral vector-based shRNA system to knock down the expression of *Lgr4* (Lgr4sh1 and Lgr4sh2) in murine MLL-AF9-HSPC pre-LSCs, which were generated by transducing an HSC-enriched hematopoietic stem/progenitor cell population (HSPCs or LSK: Lin⁻Sca-1⁺c-Kit⁺) with lentivirus encoding the MLL-AF9 fusion oncogene. MLL-AF9 serves as an initiating oncogenic event to promote self-renewal and a myeloid differentiation block in normal HSPCs and MLL-fusion oncogenes are critically dependent on β -catenin activity (Krivtsov et al., 2006; Wang et al., 2010; Yeung et al., 2010). Efficient depletion of Lgr4 protein substantially reduced expression of endogenous β -catenin, as well as several key WNT/self-renewal target genes including *c-Fos*, *Tcf7l2*, *Ccnd1* and *Mef2c*, whereas overexpression of a constitutively active form of β -catenin (β -cat*) (Wang et al., 2010) rescued the defect in colony formation caused by Lgr4 depletion (**Figures 1A-1D** and **S1B**). This provides evidence supporting WNT/ β -catenin targets as essential components downstream of LGR4 signaling.

To define a direct role of LGR4 in LSC regulation and AML development, MLL-AF9-HSPC Lgr4sh pre-LSCs were transplanted into sublethally irradiated C57BL/6 (BL6) syngeneic recipient mice. Our results showed that only 2 out of 13 (15%) mice that received Lgr4sh1 pre-LSCs and 4 out of 13 (30%) mice that received Lgr4sh2 pre-LSCs developed AML, while all control mice succumbed to primary AML with a short latency (**Figure 1E**). These data suggest that inhibition of Lgr4 impairs the initiation and progression of HSPC-derived MLL-AF9 AML in mice. Furthermore, LGR4 depletion inhibited the ability of pre-LSCs

to expand in mouse BM and to infiltrate into the spleen, evidenced by decreased percentages of GFP⁺ leukemic cells in these organs as well as lower spleen weights (**Figures 1F** and **S1C**). Morphological analysis of BM smears only exhibited abnormal immature blasts in scrambled control (Scr), whereas both leukemic blasts and differentiated myeloid cells (e.g., neutrophils) were observed in Lgr4-deficient leukemic cells indicating Lgr4 depletion-induced differentiation (**Figure 1G**). LSCs might have been severely compromised by Lgr4 depletion during development since LSCs (Lin⁻Sca-1⁻c-Kit^{high}CD16/32^{high}CD34⁺) (Krivtsov et al., 2006) flow-sorted from the BM of primary AML lacked the ability to expand in methylcellulose (data not shown). GFP⁺ Lgr4-deficient leukemic cells from primary AML could only transiently expand in the mouse BM with a reduced proliferative capacity, as determined by *in vivo* BrdU cell proliferation assays at 10 days post-transplantation, but eventually failed to induce secondary leukemia (**Figures 1H** and **1I**). In contrast, control leukemic cells could be efficiently expanded in the mouse BM and developed AML with a shorter latency in secondary recipients compared with primary engrafted mice (**Figures 1H**, **1I** and **1E**). Upon sacrifice of Lgr4sh1 and Lgr4sh2 secondary recipients at 122 days after transplantation, GFP⁺ leukemic cells were not detectable by flow cytometry in both BM and spleen (data not shown). Thus, inhibition of Lgr4 has potent leukemia-inhibitory effects and prevents the development of HSPC-derived MLL-AF9 AML *in vivo*.

To determine whether the cell of origin influences the dependence of pre-LSCs on Lgr4 signaling, we generated pre-LSCs originating from more committed progenitors by transducing MLL-AF9-GFP into granulocyte-macrophage progenitors (GMPs: Lin⁻Sca-1⁻c-Kit⁺CD16/32⁺CD34⁺) (Krivtsov et al., 2006), which expressed relatively lower levels of Lgr4 than HSPCs (**Figure S1D**). Unlike Lgr4 depletion in MLL-AF9-HSPC pre-LSCs, which caused a substantial decrease in WNT/self-renewal target genes (**Figure 1C**), knockdown of Lgr4 in MLL-AF9-GMP pre-LSCs did not significantly alter the expression of *c-Fos* but had a lesser though still significant effect on expression of *Tcf7l2*, *Ccnd1* and *Mef2c* as well as endogenous β -catenin (**Figures 1J** and **S1E**). Lgr4 depletion in MLL-AF9-GMP pre-LSCs resulted in delayed disease onset and extended survival as well as blast cell differentiation (e.g., neutrophils) and a

reduced ability of pre-LSCs to expand in mouse BM; however it had no influence on spleen weights and pre-LSC infiltration into spleen (**Figures 1K-1M** and **S1F**). In addition, unlike the potent anti-proliferative effect of *Lgr4* depletion on GFP⁺ HSPC-derived leukemic cells *in vivo*, *Lgr4* depletion revealed negligible inhibitory effect on the engraftment of GFP⁺ GMP-derived MLL-AF9 leukemic cells in the mouse BM at 10 days post-transplantation (**Figure 1N**). As a result, *Lgr4*-deficient GMP-derived leukemic cells were capable of engrafting secondary recipients with a slightly prolonged leukemia latency in mice, indicative of perhaps partially impaired LSC self-renewal (**Figure 1O**).

Our results demonstrate that dependency on LGR4 signaling may rely largely on the abundance of endogenous LGR4 expression in MLL-AF9 pre-LSCs at the initial stage of LSC development. HSPC-derived AML exhibiting higher LGR4 expression requires LGR4 for LSC functions and leukemia progression; on the other hand, GMP-derived AML has a partial requirement for LGR4. Thus, the cell of origin contributes to tumor heterogeneity in AML by determining functional effects of LGR4 on LSC self-renewal.

LGR4 cooperates with HOXA9/MEIS1 producing a highly aggressive short latency AML

HOXA9 and MEIS1 are considered to be critical targets in MLL-rearranged leukemias. Coexpression of these genes in normal HSPCs induces AML although with a less aggressive phenotype compared with MLL-AF9 in murine models (Dietrich et al., 2014; Krivtsov et al., 2006; Wang et al., 2010). Intriguingly, we observed a positive correlation between expression of *LGR4* and *HOXA9* in 183 human AML patient samples (**Figure 2A**; $r=0.546$, $p < 0.0001$) (Cancer Genome Atlas Research, 2013). This implies a potential cooperative role for LGR4 in HOXA9-mediated transformation.

To confirm this, we generated HOXA9/MEIS1 pre-LSCs by transforming LSK or GMP cells with HOXA9-GFP and MEIS1-puro followed by transduction with *Lgr4*. HOXA9/MEIS1-HSPC pre-LSCs expressed relatively lower protein levels of *Lgr4* and β -catenin compared with MLL-AF9-HSPC pre-LSCs (**Figure 2B**). We found that *Lgr4* itself was not able to fully transform normal HSPCs (data not

shown) or HOXA9/MEIS1(A9M)-transduced GMP (**Figures 2C and 2D**), but instead could cooperate with HOXA9/MEIS1 in HSPCs to accelerate disease onset and produce leukemia with shortened latencies similar to those in MLL-AF9-HSPC AML (**Figure 2E**). The enhanced aggressive phenotype in HOXA9-driven AML might be caused by an Lgr4^{OE}-induced increment in proliferation capacity *in vivo*, as we observed a 5-fold increase in GFP⁺ leukemic cells observed in the BM at 1-month post- transplantation of pre-LSCs into BL6 recipient mice, as well as by an Lgr4^{OE}-mediated increase in the quiescent (G₀) stem-like population accompanied by a decrease in intracellular ROS levels in the BM of primary AML (**Figures 2F-2H**). Western blot analysis confirmed that Lgr4 overexpression in GFP⁺ HOXA9/MEIS1 leukemic BM cells upregulated endogenous β-catenin, reaching a level similar to that in GFP⁺ MLL-AF9 leukemic BM cells (**Figure 2I**). These data are in line with elevated basal levels of LGR4 in HSPCs cooperating with HOXA9/MEIS1 to promote leukemia in mice that mirrors the full-blown aggressive MLL-AF9 AML phenotype.

Consistent with our observations in murine models, overexpression of LGR4 substantially increased tumor aggressiveness and reduced survival in NOD.Cg-Prkdc^{scid} Il2rg^{tm1Wjl}/SzJ (NSG) mice xenotransplanted with human MLL-AF9 AML cell line (THP-1) and this was associated with elevated levels of non-phosphorylated (active) β-catenin in human CD33⁺ myeloid cells from the BM of primary recipients (**Figures S2A-S2C**). Despite abundant expression of *LGR4* in both THP-1 cells and the human BCR-ABL-positive chronic myeloid leukemia (CML) K562 cell line, depletion of LGR4 decreased tumorigenesis and increased survival of THP-1 xenograft mice, but did not affect survival in K562 xenograft mice (**Figures S2D-S2F**). The difference in LGR4 function could largely be attributed to endogenous expression of *HOXA9*, which was substantially higher in THP-1 cells but absent in K562 cells (**Figure S2D**).

We found that expression levels of HOXA9 affected LGR4 function. Analysis of a published microarray dataset (Faber et al., 2009) supports this notion, showing that depletion of *HOXA9* with shRNA caused a significant decrease in expression of *LGR4*, *MEF2C* and *MEIS1* in human MLL-AF9 AML cell line

(MOLM-14) (**Figure 2J**). *Lgr4* depletion prolonged survival in HOXA9/MEIS1-HSPC mice, albeit to a much lesser extent than that in MLL-AF9-HSPC mice (**Figures 1E and 2K**). Immunophenotypic analysis revealed reduced Gr-1^{-low}c-Kit^{high} LSC-enriched population and induced differentiation (e.g., neutrophils) by *Lgr4*-depletion in HOXA9/MEIS1 leukemic BM cells (**Figures 2L and 2M**). We have previously documented that the Gr-1^{-low}c-Kit^{high} population is over 100-fold enriched for LSCs as compared with the Gr-1⁺c-Kit^{high} population in the heterogeneous LSC pool of HOXA9/MEIS1-HSPC AML (Wang et al., 2010). These results underscore an active and cooperative role of LGR4 in supporting HOXA9-dependent leukemogenesis.

LGR4 expression is upregulated by an epigenetic mechanism in human AML cell lines

HOXA9 and MEIS1 are reportedly upregulated by DOT1L-mediated H3K79 methylation in aggressive leukemia driven by oncogenes such as MLL-AF9, MLL-AF10 and CALM-AF10 (Bernt et al., 2011; Chen et al., 2013). High levels of H3K79 methylation at the loci of HOXA9 and MEIS1 are associated with high expression levels of these genes. To understand how LGR4 expression is regulated, we analyzed two independent ChIP-seq datasets for occupancy profiles of H3K79me2 and our analysis displayed the enrichment of H3K79me2 on the loci of *HOXA9*, *MEIS1*, *LGR4* and *MEF2C* in human MLL-AF9 AML (MOLM-13) cells but not in human promyelocytic leukemia (HL-60) cells, which expressed relatively low levels of *LGR4* and *HOXA9* (**Figures S2D, S3A and S3B**).

Likewise, an analysis of microarray dataset revealed that DOT1L inhibitor EPZ004777, which decreased H3K79me2 levels (Daigle et al., 2011), substantially reduced expression of *HOXA9*, *MEIS1*, *LGR4* and *MEF2C* in MOLM-13 cells (**Figure S3C**). Our results confirmed the findings and showed that DOT1L inhibitor SGC0946, which reduced H3K79me2, induced suppression of *HOXA9*, *LGR4* and *MEF2C* expression in MOLM-13 and THP-1 cells, as well as in hCD33⁺ AML PDX cells, but not in HL-60 cells (**Figures S3D-S3G**). It is thus likely that driver mutations (e.g., MLL-AF9) upregulate *LGR4* expression, at least in part, through DOT1L-mediated H3K79 methylation, which is well known for active transcription of target genes in aggressive AML (Bernt et al., 2011; Chen et al., 2013).

Inhibition of LGR4 blocks RSPO3 function in murine pre-LSCs and primary AML PDX model

LGR4 functions as a receptor of R-spondin ligands (RSPO1-RSPO4), which are potent WNT signal enhancers (Kazanskaya et al., 2004; Kim et al., 2005). Our data showed that RSPO or WNT3 alone was not sufficient to enhance endogenous β -catenin expression in murine pre-LSCs induced by MLL-AF9 or HOXA9/MEIS1 (**Figures S4A-S4F**). We found that only a combination of WNT3 and RSPO2/RSPO3 exclusively increased endogenous β -catenin expression; conversely, the combination of WNT3 and RSPO1/RSPO4 did not affect β -catenin levels (**Figures S4A-S4C**). Increasing concentrations of RSPO3 (50-200 ng/mL) or WNT3 (10-20% v/v) did not elevate β -catenin expression (**Figures S4D-S4F**). Importantly, inhibition of *Lgr4* completely abrogated RSPO3/WNT3-mediated β -catenin activation (**Figure S4G**), indicating a crucial role for LGR4 in relaying the RSPO signal to exert downstream oncogenic effects.

We next validated the above findings in a clinically relevant AML patient-derived xenograft (PDX) mouse model using CRISPR/Cas9 technology to knock out LGR4. The AML PDX model was established by xenotransplanting NSG mice with primary human AML cells from a relapsed patient harboring mutations in DNMT3A, RUNX1, KRAS, NRAS, PTPN11, ETV6 and BCOR (**Table S1**). AML PDX cells expressed high levels of *LGR4* and *HOXA9* (**Figure 3A**). LGR4 and non-phospho (active) β -catenin were predominantly expressed in the hCD34⁺ HSPC population compared with the hCD34⁻ compartment in AML PDX BM cells (**Figures 3B** and **S4H**), implicating a possible role for LGR4 in regulating human leukemia-initiating cells in primary AML. CRISPR/Cas9-mediated knockout of *LGR4* not only markedly decreased nuclear active β -catenin and consequently reduced leukemia burden in firefly luciferase (FLuc)-expressing AML PDX mice monitored by *in vivo* bioluminescence imaging, but also blocked RSPO3/WNT3-induced increase in hCD34⁺ immature cells *ex vivo* (**Figures 3C-3E, S4I** and **S4J**). These findings support the clinical relevance of LGR4 oncogenic function and underscore the importance of RSPO-LGR4 signaling in sustaining primary human hCD34⁺ immature cells.

RSPO2/3 serve as stem cell growth factors to sustain the differentiation block in AML patient blasts *ex vivo*, whereas anti-RSPO3 antibody reduces leukemia burden in NSG mice engrafted with primary AML patient specimens

Primary AML patient blasts depend on external signals such as growth factors and cytokines from the BM niche for survival and growth (Konopleva and Jordan, 2011); thus, these immature cells are difficult to culture and will differentiate if necessary and sufficient signals are not received. Given our observation that RSPOs as secreted growth factors potentiated WNT/ β -catenin activation required for LSC development, we investigated the ability of exogenous RSPO proteins to maintain primary AML blasts in their undifferentiated, immature state. We found that LGR4/HOXA9-coexpressing patient blasts were predominantly dependent on RSPO/WNT3 pathway activation and could be grown *ex vivo* in the presence of exogenous RSPO2/3 and WNT3 ligands (**Figures 4 and S5A-S5D**).

In this study, we first performed qPCR analysis on 16 primary AML patient samples and identified 5 patient specimens coexpressing *LGR4* and *HOXA9* (**Figure 4A**). Our data showed that 8 out of 16 (50%) samples expressed high levels of *LGR4*, while 5 out of 8 LGR4-expressing samples revealed relatively high levels of *HOXA9* (**Figure 4A**). We next assessed the impact of endogenous HOXA9 expression on the response of LGR4-expressing patient blasts to RSPO/WNT3 ligands. Seven LGR4-expressing patient specimens (i.e., 5 with high *HOXA9* and 2 with low *HOXA9*) were cultured under four different conditions, including medium only, cytokines (a cocktail consisting of stem cell factor, FLT3 ligand, thrombopoietin, IL-3 and IL-6), RSPO2/WNT3 or RSPO3/WNT3 (**Figure 4B and Table S2**). AML blasts in all seven LGR4-expressing patient specimens retained the immature phenotype accompanied with increased human CD34⁺ cells in cytokines, but rapidly differentiated in medium only (**Figures S5A-S5G**). Unlike cytokines that functioned irrespective of HOXA9 expression, RSPO/WNT3 ligands sustained an immature blast-like phenotype only in *LGR4/HOXA9*-coexpressing AML patient specimens, such as those harboring 9p deletion or MLL rearrangements (MLL-AF1q, MLL-AF9 or MLL-AF10), but did not maintain the undifferentiated, proliferating state in AML patient specimens with normal karyotype or harboring AML1-ETO that lacked *HOXA9*, albeit with high levels of *LGR4* expression (**Figures 4B, 4C, S5A-S5G and**

Table S2). These observations not only support a cooperative function of HOXA9 in RSPO-LGR4 pathway activation, but also underline the role of RSPO2/3 as growth factors that increase proliferation and preserve the immature stem cell-like phenotype of primary human AML patient blasts.

Notably, anti-RSPO3 monoclonal antibody (OMP-131R10/rosmantuzumab; OncoMed Pharmaceuticals), which has proven to be safe and well tolerated in Phase 1 clinical trials in advanced solid tumors, blocked RSPO3/WNT3-induced increase of human CD34⁺ immature blasts in primary AML patient specimens and PDX cells, phenocopying the inhibitory effect of *LGR4* knockout in AML PDX cells (**Figures 3D, S5A and S6A-S6B**). The anti-RSPO3-induced phenotype was associated with suppression of endogenous *LGR4* and *HOXA9* expression (**Figure S6C**). Altogether, these findings uncover a critical dependency of LGR4/HOXA9-coexpressing primary human AML cells on RSPO/WNT3 ligands for their growth and survival, implicating anti-RSPO3 antibody as a potential therapeutic agent for AML treatment.

We next examined the *in vivo* therapeutic potential of anti-RSPO3 antibody by treating NSG mice engrafted with primary AML patient specimens (**Figure 4D**). Among five AML patient specimens coexpressing LGR4 and HOXA9, three harboring 9p deletion, MLL-AF9 or MLL-AF1q were successfully engrafted consistent with an approximate 50% engraftment rate of primary AML patient samples in NSG mice (Krevvata et al., 2018). In line with our *ex vivo* observations, all three engrafted patient specimens responded to anti-RSPO3 antibody treatment *in vivo*, resulting in markedly decreased percentages of human CD34⁺CD45⁺ LSC-enriched cells as well as reduced spleen weight and size in NSG mice (**Figures 4E-4G and S6D-S6F**). Likewise, *in vivo* anti-RSPO3 treatment significantly reduced expression of endogenous *LGR4* and *HOXA9* (**Figure S6E**). These findings support the therapeutic value of anti-RSPO3 antibody for targeting primary patient cells in the treatment of AML dependent on HOXA9, an indicator of poor prognosis.

Clinical-grade anti-RSPO3 antibody targets LSC-enriched populations in AML PDXs but not normal human HSPCs in NSG mice

Consistent with our *in vivo* observations of primary AML patient samples directly engrafted in NSG mice,

the established PDX model of primary AML responded to anti-RSPO3 antibody treatment, which markedly reduced leukemia burden and diminished the percentage of hCD34⁺ cells in mouse BM (**Figures 5A and 5B**). The anti-RSPO3-response was primarily attributable to a substantial decrease in nuclear active β -catenin and several key WNT/self-renewal target genes including *c-FOS*, *TCF7L2*, *CCND1*, *MEF2C* and HOX cluster genes *HOXA7* and *HOXA11* in hCD34⁺ cells, as well as induced differentiation of hCD33⁺ myeloid blasts (**Figures 5C-5E**). Subsequent *in vivo* serial transplantation showed that hCD33⁺ myeloid blasts isolated from anti-RSPO3-treated primary mice failed to engraft into secondary NSG recipients (**Figure 5F**), indicating anti-RSPO3-induced functional impairment in the LSC compartment in the PDX mouse model of primary human AML.

In contrast to the observation in AML PDX mice, anti-RSPO3 treatment (20 mg/kg, i.p., once per week for 5 weeks) had negligible growth-inhibitory effects in NSG mice engrafted with expanded normal human CD34⁺ HSPCs (**Figures 5G and S7A-S7D**), which could be a consequence of intrinsic relative LGR4 independence. Collectively, we conclude that the anti-RSPO3 antibody selectively targets CD34⁺ LSC-enriched populations in primary human AML and has potential as a therapeutic agent for the treatment of leukemias, which rely on RSPO-LGR4 activation associated with coexpression of LGR4 and HOXA9.

RSPO-LGR4 upregulates key WNT/self-renewal target genes through the pCREB-CBP pathway

We next investigated how RSPO-LGR4 regulates WNT/self-renewal target genes. G protein-coupled receptors often activate downstream signaling pathways through their coupled G protein subunits. We found a strong correlation between expression of *LGR4* and *GNAS* in 1064 AML patient samples irrespective of their subtypes, by analyzing an integrated gene expression dataset of five independent studies (**Figure 6A**; $r=0.789$, $p < 0.0001$; GSE13159, GSE15434, GSE61804, GSE14468 and The Cancer Genome Atlas TCGA) (Bagger et al., 2016). In agreement with this observation, overexpression of G protein alpha-subunit $G_{\alpha s}$ (encoded by *GNAS*) not only increased non-phospho (active) β -catenin to the level similar to that induced by RSPO2/WNT3 in human MLL-AF9 AML (THP-1) cells, but also

substantially augmented RSPO2/WNT3-induced activation of β -catenin (**Figure 6B**). Conversely, G_{α_s} knockdown with GNAS shRNAs reduced the level of active β -catenin (**Figures 6C and S8A**). These results indicate an active involvement of G_{α_s} in RSPO-LGR4 signaling.

G_{α_s} has a known function in cAMP-dependent pathway activation. The cAMP-Glo assay and western blot analyses showed that RSPO2/WNT3 stimulation significantly elevated the intracellular cAMP level (**Figure S8B**), which increased phosphorylation of nuclear transcription factor CREB (cAMP-response element binding protein) at Ser133 in human MLL-AF9 THP-1 cells (**Figures 6D**). LGR4 depletion resulted in a marked decrease in p-CREB^{Ser133}, which is an active transcriptional form (**Figure 6E**). Knockdown of CREB with shRNAs resulted in reduced levels of p-CREB^{Ser133} and decreased expression of both active and total β -catenin (**Figures 6F and S8C**). The phosphorylation of CREB is associated with poor survival and increased risk of relapse in AML patients (Shankar et al., 2005). Elevated nuclear p-CREB^{Ser133} was observed in hCD33⁺ AML PDX cells; conversely, *in vivo* anti-RSPO3 treatment inhibited phosphorylation of nuclear CREB in hCD34⁺ cells isolated from the BM of treated AML PDX mice (**Figures 6G and 6H**). The phosphorylation event enables CREB to bind to and recruit histone acetyltransferases CBP (CREB-binding protein) and its paralog p300, which induce acetylation of nuclear transcription factors (e.g., β -catenin) to activate downstream target genes (Chrivia et al., 1993; Hoffmeyer et al., 2017).

In agreement with the inhibitory effect of *LGR4* knockout or anti-RSPO3 treatment in AML PDXs (**Figures 3C and 5**), we observed that treatment with I-CBP112, a selective inhibitor of the CBP/p300 bromodomain, triggered cell differentiation and blocked RSPO3/WNT3-induced increase in hCD34⁺ immature cells (**Figures 6I and S8D**). The I-CBP112-induced deficient phenotype was associated with significantly decreased expression of key WNT/self-renewal target genes including *MEIS1*, *MEF2C*, *CCND1* and HOX cluster genes *HOXA7*, *HOXA9* and *HOXA11*, as well as β -catenin transcriptional cofactors *c-FOS* and *TCF7L2* in AML PDX cells (**Figure 6J**). Collectively, these data suggest that RSPO-LGR4 regulates WNT/self-renewal target genes, at least partially, through the pCREB-CBP pathway in

human AML. We cannot rule out the possibility that LGR4 activates pathways in addition to pCREB-CBP. Thus, blocking the RSPO3-LGR4 interaction by anti-RSPO3 antibody is superior to targeting pathways downstream of LGR4 for the therapeutic purpose.

DISCUSSION

AML is a highly heterogeneous and aggressive malignancy initiated with the formation of pre-LSC clones through a range of initiating oncogenic events (e.g., recurrent mutations, gene fusions involving the MLL gene, elevated HOXA9/MEIS1), resulting in an aberrant self-renewal program and providing a selective growth advantage over their origin (e.g., HSPCs, GMPs) (Cozzio et al., 2003; Krivtsov et al., 2006; Welch et al., 2012). Each pre-LSC may acquire different additional cooperating event(s) (e.g., increased WNT/ β -catenin, DOT1L-mediated H3K79 methylation), enabling pre-LSCs to further transform into a heterogeneous LSC pool with enhanced self-renewal activity (Bernt et al., 2011; Krivtsov et al., 2006; Wang et al., 2010; Yeung et al., 2010). Given that persistent LSCs are a major cause of treatment failure and relapse that occurs frequently for certain aggressive AML subtypes, understanding the transformation process and pharmacologically tractable pathways that sustain the LSC pool is of crucial importance for the design of effective cancer therapies.

Previous studies have shown that the cell of origin is an important factor controlling disease phenotype and clinical outcome in AML, where pre-LSCs originated from HSPCs develop a more aggressive subtype of AML than do those originated from GMPs serving as a reservoir of disease in patients with poor survival (Krivtsov et al., 2013; Stavropoulou et al., 2016). Likewise, our results indicate that LSCs derived from HSPCs appear to rely heavily on LGR4 signaling for self-renewal and the establishment of a particularly aggressive phenotype in mice; conversely, LSCs derived from GMPs exhibit only a partial dependency on LGR4 signaling. It is likely that LSCs developed from different origins utilize distinct endogenous signaling mechanisms driving tumorigenesis. We have previously shown that G_{aq} signaling is required for the maintenance of GMP-derived MLL-AF9 AML, and genetic and pharmacological blockade of G_{aq} suppresses β -catenin activity leading to impaired leukemogenesis via inhibition of

mitochondrial energy metabolism and activation of GADD45a-associated stress response (Lynch et al., 2016). Notably, recent studies demonstrate a direct link between LGR4 and Ga_q signaling where LGR4 relays signals via coupling to Ga_q during osteoclastogenesis (Luo et al., 2016). Thus, GMP-derived MLL-AF9 AML may require co-activation and cooperation of multiple signaling pathways including LGR4 and Ga_q to maintain β -catenin activity and self-renewal. In support of this notion, we observe that overexpression of LGR4 in GMP-derived HOXA9/MEIS1 pre-LSCs increases leukemia incidence but does not significantly affect the survival rate in mice; this is different from the potent pro-oncogenic effect of LGR4 in HSPC-derived HOXA9/MEIS1 AML, indicating additional upstream molecules contributing to the activation of β -catenin required for GMP transformation via HOXA9/MEIS1. Our findings underline the importance of identifying key regulatory elements upstream of β -catenin signaling as they have the capacity to manipulate downstream signal events that determine origin-specific tumorigenic effects. The origin-dependent difference in pathway requirements contributes to the heterogeneity of the LSC pool within a tumor.

The mechanism underlying the enhanced aggressive leukemia phenotype associated with elevated LGR4 may involve functional cooperation between LGR4 and HOXA9 in LSCs. High levels of HOXA9 expression is a characteristic feature of AML, including cases with MLL rearrangements, and is associated with poor clinical outcome (Golub et al., 1999). We have previously demonstrated that enforced expression of HOXA9/MEIS1 transforms normal HSPCs where β -catenin is normally active, but is not able to fully transform GMPs that inherently lack β -catenin activity and self-renewal ability (Wang et al., 2010). This implicates an indispensable requirement for β -catenin activation in HOXA9-mediated transformation. Consistent with the role of β -catenin in promoting LSC self-renewal and the role of LGR4 as an essential upstream effector of β -catenin signaling, we observe that LGR4 cooperates with HOXA9/MEIS1 in HSPCs contributing to a highly tumorigenic phenotype characteristic of MLL-AF9 AML. This is in line with a positive correlation between the expression of *LGR4* and *HOXA9* in AML patient samples and the observation that coexpression of *LGR4* and *HOXA9* is a necessary prerequisite for RSPO-LGR4 oncogenic activity in primary AML patient specimens. Thus, functional cooperation between

LGR4 activation and a HOXA9 gene expression program likely drives *in vivo* self-renewal and enhanced leukemogenesis.

Here we report a differential requirement of RSPO-LGR4 signaling between LSCs and normal HSCs. Previous studies have demonstrated that the WNT ligand itself is sufficient to activate canonical WNT/ β -catenin signaling in normal HSCs, by forming a ternary complex with the LRP5/6 and Frizzled receptors (Reya et al., 2003; Tamai et al., 2000; Willert et al., 2003). Our findings add support to this notion, showing that *in vivo* anti-RSPO3 antibody treatment has negligible inhibitory effect on engraftment of normal human CD34⁺ HSPCs in xenotransplanted mice. In contrast to normal HSCs, we uncover that WNT activation of β -catenin in primary AML critically depends on a second signal provided by an RSPO ligand that drives the self-renewal of LSCs through an LGR4-dependent mechanism. RSPO-LGR4 reportedly forms a supercomplex with the WNT receptors and consequently enhances β -catenin signaling by synergizing with low levels of the WNT ligand (de Lau et al., 2011). The potency of RSPOs in enhancing WNT signals is not affected by WNT receptor levels, but instead largely depends on the abundance of LGR expression (de Lau et al., 2011). We show that pharmacological disruption of the RSPO-LGR4 interaction by clinical-grade anti-RSPO3 antibody decreases leukemia burden in AML patient-derived xenografts and impairs engraftment of secondary recipients consistent with effective targeting of LSCs. This treatment shows negligible impact on normal human stem cell compartment in NSG mice. While the therapeutic efficacy of anti-RSPO3 antibody will need further preclinical validation in a large number of PDX models with varying mutational profiles, our findings indicate differential dependence of normal and malignant stem cells on RSPO-LGR4 signaling, and suggest that LGR4 levels may provide a biomarker for anti-RSPO3 antibody treatment and that a therapeutic window exists for selective targeting of LSCs.

Overall, our studies have elucidated unique properties of AML LSCs that drive particularly aggressive disease and define a critical role for RSPO-LGR4 signaling in promoting β -catenin activation and AML leukemogenesis. Aberrant activation of RSPO-LGR4 is essential for sustaining self-renewal and a myeloid

differentiation block, which contribute to the aggressive leukemia phenotype through cooperation with HOXA9. LGR4 depletion and anti-RSPO3 antibody treatment compromise LSCs and impede AML initiation in both murine models and patient-derived xenografts, underscoring the therapeutic value of targeting RSPO-LGR4 signaling in AML.

Figure 1. Inhibition of LGR4 exerts origin-specific blockade of aberrant self-renewal and AML progression in mice.

(A) Schematic outline of the experimental procedure.

(B) Western blots confirming sufficient knockdown of *Lgr4* and a resultant reduction of endogenous β -catenin protein in MLL-AF9-HSPC pre-LSCs carrying scrambled control (Scr) versus *Lgr4* shRNAs.

(C) qPCR showing relative expression levels of key Wnt/self-renewal target genes in MLL-AF9-HSPC pre-LSCs carrying Scr versus *Lgr4* shRNAs. n=3 replicates per condition.

(D) Colony formation of Scr versus *Lgr4*shRNA-expressing MLL-AF9-HSPC pre-LSCs transduced with constitutively active β -catenin (β -cat*) or empty vector (Neo). The number of colonies per dish at the 3rd round of serial replating is shown. n=3 independent experiments.

(E) Kaplan-Meier survival curves of mice receiving MLL-AF9-HSPC pre-LSCs carrying Scr versus *Lgr4* shRNAs. 1×10^6 pre-LSCs were transplanted into sublethally irradiated (6 Gy) BL6 recipient mice for the development of primary AML. n=13 mice per group. P value was determined by the log-rank test.

(F) Percentages of GFP⁺ BM cells (left panel) and spleen cells (right panel) from mice with MLL-AF9-HSPC primary AML carrying Scr versus *Lgr4* shRNAs.

(G) Wright-Giemsa staining ($\times 60$ magnification) of BM cells from mice with MLL-AF9-HSPC primary AML showing *Lgr4*-depletion-induced differentiation of leukemic blasts. Arrows indicate metamyelocytes, mature and banded neutrophils.

(H) Percentages of BrdU⁺ BM cells at 10 days post-transplantation. 1×10^5 GFP⁺ leukemic cells from primary AML were transplanted into secondary recipient mice. n=4 mice per group.

(I) Kaplan-Meier survival curves of mice receiving GFP⁺ leukemic BM cells flow-sorted from primary AML. 1×10^5 leukemic cells were transplanted into secondary recipient mice for the development of secondary AML. n=6 mice per group.

(J) qPCR showing relative expression levels of key Wnt/self-renewal target genes in MLL-AF9-GMP pre-LSCs carrying Scr versus *Lgr4*sh1. n=3 replicates per condition.

(K) Kaplan-Meier survival curves of mice receiving MLL-AF9-GMP pre-LSCs carrying Scr versus *Lgr4*sh1. 1×10^6 pre-LSCs were transplanted into sublethally irradiated (6 Gy) BL6 recipient mice for the development of primary AML. n=9 mice per group. P value was determined by the log-rank test.

(L) Wright-Giemsa staining ($\times 60$ magnification) of BM cells from mice with MLL-AF9-GMP primary AML. Arrows indicate neutrophils.

(M) Percentages of GFP⁺ BM cells (left panel) and spleen cells (right panel) from mice with MLL-AF9-GMP primary AML carrying Scr versus *Lgr4*sh1.

(N) Percentages of BrdU⁺ BM cells at 10 days post-transplantation. 1×10^5 GFP⁺ leukemic cells from primary AML were transplanted into secondary recipient mice. n=6 mice per group.

(O) Kaplan-Meier survival curves of mice receiving GFP⁺ leukemic BM cells flow-sorted from primary AML. 1×10^5 leukemic cells were transplanted into secondary recipient mice. n=5 mice per group. P value was determined by the log-rank test.

Data are represented as the mean \pm SD. Unpaired t test. * p < 0.05, ** p < 0.005, *** p < 0.0005, **** p < 0.0001; NS, not significant (p > 0.05).

See also Figure S1.

Figure 2. LGR4 cooperates with HOXA9/MEIS1 producing a highly aggressive short latency AML.

(A) Microarray data analysis of 183 AML patient samples (Cancer Genome Atlas Research Network, 2013) showing a significant positive correlation between expression of *LGR4* and *HOXA9*. p < 0.0001 and

$r = 0.546$.

(B) Western blots revealing higher levels of endogenous Lgr4 and β -catenin proteins in MLL-AF9- HSPC pre-LSCs than in HOXA9/MEIS1 (A9M)-HSPC pre-LSCs.

(C) Western blots confirming overexpression of Lgr4 (Lgr4^{OE}) in A9M-GMP pre-LSCs transduced with MSCV-Lgr4-neo.

(D) Kaplan-Meier survival curves of mice receiving neo versus Lgr4^{OE} A9M-GMP pre-LSCs. 1×10^6 pre-LSCs were transplanted into sublethally irradiated BL6 recipient mice for the development of primary AML. n=12 mice per group. P value was determined by the log-rank test.

(E) Kaplan-Meier survival curves of mice receiving neo versus Lgr4^{OE} A9M-HSPC pre-LSCs (n=9 mice per group) or MLL-AF9-HSPC pre-LSCs (n=6 mice). 1×10^6 pre-LSCs were transplanted into sublethally irradiated BL6 recipient mice for the development of primary AML. P value was determined by the log-rank test.

(F) Representative flow cytometry dot plots illustrating *in vivo* proliferation of neo versus Lgr4^{OE} GFP⁺ A9M-HSPC pre-LSCs in mouse BM at 1-month post-transplantation. 1×10^6 pre-LSCs were transplanted into sublethally irradiated BL6 recipient mice. Scatter dot plots represent the mean \pm SD. n=3 mice per group. Unpaired t test. **** p < 0.0001.

(G) Cell cycle analysis of neo versus Lgr4^{OE} GFP⁺ A9M-HSPC leukemic BM cells. Percentages of cells in G₀ (Ki-67⁻7AAD⁻) are shown (n=3 independent experiments). Scatter dot plots represent the mean \pm SD. Unpaired t test. * p < 0.05.

(H) Representative histogram showing the level of intracellular ROS in neo versus Lgr4^{OE} GFP⁺ A9M-HSPC leukemic BM cells.

(I) Western blots showing endogenous β -catenin expression in neo versus Lgr4^{OE} A9M-HSPC and MLL-AF9-HSPC GFP⁺ leukemic BM cells.

(J) Analysis of a published microarray dataset (Faber et al., 2009) showing *HOXA9* knockdown-induced decrease in expression of *LGR4*, *MEF2C* and *MEIS1* in human MLL-AF9 AML (MOLM-14) cells (n=6 samples per condition).

(K) Kaplan-Meier survival curves of mice receiving A9M-HSPC pre-LSCs carrying Scr versus Lgr4sh1. 2×10^6 pre-LSCs were transplanted into sublethally irradiated BL6 recipient mice for the development of primary AML. n=11 mice per group. P value was determined by the log-rank test.

(L) Percentages of Gr-1⁻c-Kit^{high} population in A9M-HSPC BM cells from primary AML (Scr, n=3 mice; Lgr4sh1, n=4 mice). Scatter dot plots represent the mean \pm SD. Unpaired t test. * p < 0.05.

(M) Wright-Giemsa staining ($\times 60$ magnification) of BM cells from mice with A9M-HSPC primary AML showing Lgr4-depletion-induced differentiation of leukemic blasts. Arrows indicate neutrophils.

See also Figures S2 and S3.

Figure 3. LGR4 knockout blocks RSPO3 signal and reduces tumor burden in a primary AML PDX model.

(A) qPCR showing increased expression levels of *LGR4* (left panel) and *HOXA9* (right panel) in hCD33⁺ myeloid cells isolated from primary human AML PDX mice, compared with normal human hCD34⁺ HSPCs and hCD33⁺ remission samples obtained from AML patients with normal karyotype. Mean \pm SD. n=3 replicates per sample. **** p < 0.0001. One-way ANOVA.

(B) Representative IF images revealing increased nuclear active non-phospho β -catenin in hCD34⁺ PDX cells compared with the hCD34⁻ compartment. Scale bar, 10 μ m.

(C) Schematic describing *in vivo* generation of CRISPR/Cas9-mediated knockout (KO) of *LGR4* in PDX mice.

(D) Absolute numbers of viable hCD34⁺ immature cells from CRISPR-Cas9-non-targeting control (CRISPR-Ctr) versus *LGR4* KO primary AML PDX cells after 24 h of culture with 200 ng/mL human RSPO3/WNT3. Scatter dot plots represent the mean \pm SD. n=3 replicates. Unpaired t test. ** p < 0.005.

(E) *In vivo* bioluminescence imaging and total flux (photons/sec; p/s) for CRISPR-Ctr versus *LGR4* KO PDX mice. See **Figure S4I** for experimental details. Scatter dot plots represent the mean \pm SD. n=3 mice per group. Unpaired t test. ** p < 0.005.

See also Figure S4 and Table S1.

Figure 4. RSPO2/3 serve as stem cell growth factors to sustain differentiation block of primary AML patient blasts *ex vivo* while anti-RSPO3 antibody treatment reduces leukemia burden in NSG mice directly engrafted with primary AML patient specimens.

(A) qPCR showing relative expression levels of *LGR4* (n=16 AML patient specimens) and *HOXA9* (n=8 AML patient specimens) in primary AML patient specimens with various cytogenetics abnormalities, compared with normal human CD34⁺ HSPCs. Data are represented as the mean \pm SD. n=3 replicates per AML patient specimens. * p < 0.05, ** p < 0.005, **** p < 0.0001; NS, not significant (p > 0.05). One-way ANOVA.

(B) Schematic overview of AML patient samples responding to RSPO/WNT ligand stimulation *ex vivo*.

(C) Wright-Giemsa staining ($\times 60$ magnification) of primary AML patient specimen harboring MLL-AF9, after 48 h of culture in indicated media conditions. Scale bar, 20 μ m.

(D) Schematic describing generation of PDX mouse models by engrafting NSG mice with primary AML patient specimens harboring 9p deletion (7×10^6 cells per mouse), MLL-AF9 (1.6×10^6 cells per mouse) or MLL-AF1q (5.7×10^6 cells per mouse), followed directly by *in vivo* treatment with control versus anti-RSPO3 antibodies (20 mg/kg, i.p. every 4 days). *Note:* Primary AML patient specimens harboring diagnosis or relapse MLL-AF10 (7.1×10^5 or 1.7×10^6 cells per mouse) showed no engraftment in NSG mice. Indicated numbers of transplanted patient cells were determined by their availability in our patient tumor bank and equal numbers of patient cells were transplanted in control versus anti-RSPO3 treatment groups for each patient specimen.

(E) Percentages of human CD34⁺CD45⁺ LSC-enriched subpopulations in the BM of NSG mice engrafted with 9p deletion patient specimen followed by *in vivo* anti-RSPO3 treatment. BM cells were harvested at 154 days post-transplantation for FACS analysis. Scatter dot plots represent the mean \pm SD. n=3 mice per group. Unpaired t test. ** p < 0.005.

(F and G) Flow cytometry plots depicting the percentage of human CD45⁺ or CD45⁺CD34⁺ leukemic cells in the BM of NSG mice engrafted with MLL-AF9 patient specimen (F) or MLL-AF1q patient specimen (G), followed by *in vivo* anti-RSPO3 treatment. BM cells were harvested from MLL-AF9 mice at 83 days post-transplantation and from MLL-AF1q mice at 159 days post-transplantation.

See also Figures S5-S6 and Table S2.

Figure 5. Clinical-grade anti-RSPO3 antibody reduces leukemia burden and compromises primary LSCs in an AML PDX mouse model but does not affect normal human HSPCs in NSG mice.

(A) *In vivo* bioluminescence imaging and total flux (p/s) of AML PDX mice treated with anti-RSPO3 antibody (20 mg/kg, i.p. once per week for 4 weeks). One mouse was excluded from further analysis as the baseline bioluminescent signal was notably higher than the cohort. ** p < 0.005. Two-way ANOVA.

(B) Percentages of hCD34⁺ cells engrafted in the BM of AML PDX mice in response to *in vivo*

anti-RSPO3 treatment. Scatter dot plots are represented as the mean \pm SD. Unpaired t test. * $p < 0.05$.

(C) Representative IF images displaying reduced levels of non-phospho (active) β -catenin in hCD34⁺ HSPCs isolated from AML PDX mice in response to *in vivo* anti-RSPO3 treatment. Scale bar, 10 μ m.

(D) qPCR showing downregulation of key WNT/self-renewal target genes in hCD34⁺ cells isolated from AML PDX mice in response to *in vivo* anti-RSPO3 treatment. Mean \pm SD. n=3 replicates per condition. Unpaired t test. **** $p < 0.0001$.

(E) Wright-Giemsa staining ($\times 60$ magnification) of hCD33⁺ cells isolated from AML PDX mice showing anti-RSPO3-induced differentiation of immature AML PDX cells. Arrows indicate metamyelocytes and neutrophils.

(F) *In vivo* Bioluminescence imaging and total flux (p/s) of secondary NSG recipient mice, which were xenotransplanted i.v. with 3×10^4 hCD33⁺ myeloid cells isolated from primary AML PDX mice treated with control versus anti-RSPO3 antibodies. *Note*: Transplanted secondary recipient mice received no further treatment. **** $p < 0.0001$. Two-way ANOVA.

(G) Percentages of normal hCD45⁺ cells engrafted in the PB and hCD34⁺ HSPCs in the BM of NSG recipient mice at 106 days post-transplantation, following *in vivo* anti-RSPO3 antibody treatment (20 mg/kg, i.p. once per week for 5 weeks). Data are represented as the mean \pm SD. n=3 mice per group. Unpaired t test. NS, not significant ($p > 0.05$).

See also Figure S7.

Figure 6. RSPO-LGR4 upregulates key WNT/self-renewal target genes through the pCREB-CBP pathway.

(A) Integrated analysis of 5 independent gene expression datasets (GSE13159, GSE15434, GSE61804, GSE14468, and The Cancer Genome Atlas TCGA) (Bagger et al., 2016) showing a strong positive correlation between expression of *LGR4* and *GNAS* in 1064 primary AML patient samples. $p < 0.0001$ and $r = 0.789$.

(B) Western blots demonstrating overexpression of V5-tagged human $G_{\alpha s}$ protein in human MLL- AF9 (THP-1) cells and resultant changes in non-phospho (active) β -catenin in response to 5 h of culture with 200 ng/mL of RSPO2/WNT3.

(C) Western blots confirming downregulation of active β -catenin caused by $G_{\alpha s}$ knockdown, which was induced by *GNAS* shRNA in human AML THP-1 cells.

(D) Western blots demonstrating RSPO2/WNT3-induced increase in p-CREB^{Ser133} relative to total CREB (tCREB) in the nuclear fraction but no change in the cytosol fraction of human THP-1 cells, following 5 h of culture with 200 ng/mL of RSPO2/WNT3. Scatter dot plots represent the band intensity as mean \pm SD. n=3 independent experiments. Unpaired t test. * $p < 0.05$; NS, not significant ($p > 0.05$).

(E) Western blots confirming downregulation of p-CREB^{Ser133} induced by *LGR4* depletion in human THP-1 cells carrying *LGR4* shRNA.

(F) Western blots confirming decreased levels of p-CREB^{Ser133}, total β -catenin and active β -catenin in human THP-1 cells carrying CREB shRNA.

(G and H) Representative IF images showing expression of nuclear active p-CREB^{Ser133} in hCD33⁺ AML PDX cells (G) and in hCD34⁺ cells (H) isolated from Ctr- versus anti-RSPO3-treated AML PDX mice. Scale bar, 10 μ m.

(I) Absolute numbers of viable hCD34⁺ immature cells from primary AML PDX cells treated with DMSO versus 1 μ M I-CBP112 for 24 h of culture with 200 ng/mL RSPO3/WNT3. Scatter dot plots represent the mean \pm SD. n=6 replicates. Unpaired t test. **** $p < 0.0001$.

(J) qPCR showing reduced levels of key WNT/self-renewal target genes in primary AML PDX cells in response to treatment with 1 μ M I-CBP112 for 24 h of culture with 200 ng/mL RSPO3/WNT3. Mean \pm SD. n=4 replicates per condition. Data are representative of at least 3 independent repeats. Unpaired t test. * $p < 0.05$, ** $p < 0.005$, *** $p < 0.0005$.

See also Figure S8.

STAR METHODS

RESOURCE AVAILABILITY

Lead Contact and Materials Availability

Further information and requests for resources and reagents should be directed to and will be fulfilled by the Lead Contact, Jenny Y. Wang (jwang@ccia.unsw.edu.au). All unique/stable reagents generated in this study are available from the Lead Contact with a completed Materials Transfer Agreement.

Data and Code Availability

This study did not generate datasets and code. Previously published expression datasets used in this study are available through GEO under GEO: GSE13714, GSE29828, GSE13159, GSE15434, GSE61804, GSE14468 as well as The Cancer Genome Atlas (TCGA). ChIP-seq datasets are available through GSM1519628 and GSE43063.

EXPERIMENTAL MODEL AND SUBJECT DETAILS

Animals

All animal studies were conducted in compliance with the Australian Code for the care and use of animals and under UNSW Animal Care and Ethics Committee approved protocols (14/123B, 17/48B and 18/1B). Female C57BL/6 (BL6) and NOD.Cg-Prkdc^{scid} Il2rg^{tm1Wjl}/SzJ (NSG) mice were obtained from Australian BioResources and used for the transplantation experiments between 6 and 8 weeks of age. Mouse models of MLL-AF9-HSPC, MLL-AF9-GMP, HOXA9/MEIS1-HSPC and HOXA9/MEIS1-GMP-driven AML as well as patient-derived and cell line-derived xenografts were established by transplanting leukemic cells into BL6 or NSG mice as previously described (Wang et al., 2010; Dietrich et al., 2014; Gonzales-Aloy et al., 2019; Lynch et al., 2019). Transplanted mice were examined regularly for ill health according to our approved protocols. The PDX model used for *in vivo* bioluminescence imaging was established by transplanting into NSG mice with firefly luciferase (FLuc)-expressing primary human AML cells from a relapsed patient harboring multiple mutations including DNMT3A, RUNX1, K/NRAS, PTPN11, ETV6 and BCOR (**Table S1**). Mice were randomly assigned into control or treatment groups.

Primary AML patient specimens

AML patient samples were obtained from the Sydney Children's Tumour Bank Network and were consented for research purpose. Ethical approval was obtained from the Sydney Children's Hospitals Network Human Research Ethics Committee. Frozen BM samples from AML patients at the time of diagnosis, relapse or remission were used under institutional review board-approved protocols. Clinical characteristics of AML patient samples with 9p deletion, MLL-AF1q, MLL-AF9, MLL-AF10 (diagnosis

and relapse), AML1-ETO and normal karyotype were summarized in **Table 1**. Normal adult human CD34⁺ BM cells were obtained from Lonza (Mt Waverley, VIC, Australia).

Cell lines

All cell lines were obtained from the sources indicated in the Key Resources Table. MOLM-13 (source: male), THP-1 (source: male), HL-60 (source: female) and K562 (source: female) cells were cultured in RPMI-1640 supplemented with 10% fetal bovine serum (FBS) and 1% penicillin/streptomycin at 37°C with 5% CO₂. HEK293T cells were used for virus production and were cultured in DMEM supplemented with 10% FBS and 1% penicillin/streptomycin. Cells were tested regularly for mycoplasma. THP-1 and MOLM-13 were authenticated using short tandem repeat profiling and other cell lines were used within 10 passages without further authentication.

METHOD DETAILS

***Ex vivo* culture of primary AML patient cells**

Primary AML patient specimens or AML PDX cells were thawed in RPMI-1640 medium (Thermo Fisher Scientific, North Ryde, NSW, Australia) and cultured in various media conditions, such as (1) medium only (RPMI-1640 supplemented with 1% FBS); (2) cytokines (StemSpan™ CD34⁺ Expansion Supplement [x10] consisting of hSCF, hFLT3-L, hTPO, hIL-3 and hIL-6; StemCell Technologies, 02691); (3) 200 ng/mL RSPO2/WNT3 in medium; (4) 200 ng/mL RSPO3/WNT3 in medium; or (5) 200 ng/mL RSPO3/WNT3 with 150 µg/mL anti-RSPO3 antibody in medium for 24-96 h. The percentage of hCD34⁺ cells in primary AML patient blasts was determined by FACS analysis using Alexa Fluor 647 anti-human CD34 (343508) from BioLegend (Balcatta, WA, Australia)

Flow-sorting and FACS analysis

Cells were stained with antibodies at 4 °C for 30 min before being subjected to flow sorting using BD Influx™ cell sorter or BD FACSAria™ III sorter (BD Biosciences, North Ryde, NSW, Australia) and to FACS analysis using BD LSRFortessa™ cell analyzer or BD FACSCanto™ II (BD Biosciences). Flow cytometry data were analyzed using FlowJo software (TreeStar, Ashland, OR, USA).

FACS analysis of human LGR4 expression

hCD34⁺ and hCD34⁻ PDX cells were fixed in 4% paraformaldehyde (PFA) for 15 min at room temperature and then permeabilized in 0.1% Triton X for 15 min. Cells were washed and subsequently stained with 2 µg/mL LGR4 primary antibody (Abcam, Melbourne, VIC, Australia; ab137480) in 3% BSA for 1 h at room temperature followed by Alexa Fluor 647-conjugated secondary antibody (Abcam; 150079) at a

dilution of 1:3000 in 3% BSA for 45 min, prior to FACS analysis.

Hematopoietic stem/progenitor cell isolation

Human CD34⁺ leukemic cells were isolated from mouse BM using EasySep™ human CD34 positive selection Kit (StemCell Technologies, Tullamarine, VIC, Australia; 18056), and human CD33⁺ leukemic cells were isolated from mouse BM using EasySep™ human CD33 positive selection Kit (StemCell Technologies, 18287), as per manufacturers' protocols. The purity (>98%) of the resulting isolated population was confirmed using FACS analysis. Murine HSC-enriched LSK cells were flow-sorted as Lin⁻(CD3, CD4, CD8a, CD19, B220, Gr-1, Ter119, IL-7R)Sca-1⁺c-Kit⁺ (BioLegend) and myeloid progenitor GMP cells were isolated as GMPs: Lin⁻Sca-1⁻c-Kit⁺CD16/32⁺CD34⁺ (BioLegend) from mouse BM as previously described (Akashi et al., 2000; Krivtsov et al., 2006).

Anti-RSPO3 monoclonal antibody

Anti-RSPO3 monoclonal antibody (OMP-131R10/rosmantuzumab; OncoMed Pharmaceuticals, CA, USA) was generated by immunizing mice with purified recombinant human RSPO3 followed by hybridoma generation and characterization (Chartier et al., 2016). The anti-RSPO3 antibody has been well tolerated as a single agent in a phase 1 clinical trial in advanced solid tumors and dose-limiting toxicities were not observed (Bendell et al., 2016).

***In vivo* treatments and analysis of tumor burden**

For the established PDX model, genetic characterization of the AML PDX was performed using a targeted, multiplexed amplicon resequencing approach (Haloplex, Agilent, Boeblingen, Germany), as described previously (Metzeler et al., 2016; Vick et al., 2015). Non-invasive bioluminescence imaging was used to monitor and assess *in vivo* engraftment of human AML cells. PDX mice were injected with D-luciferin (150 mg/kg of body weight, Xenogen, Alameda, CA) via intraperitoneal (i.p) injection. Images were subsequently taken and signal output was measured 10 min after injecting the substrate. Signal intensity quantification and analysis were performed using the Living Image software version 3.0 (Xenogen). The bioluminescent signal was recorded as radiance photons/sec/cm²/steradian (p/sec/cm²/sr), represented in pseudocolor to indicate the signal intensities. Mice were excluded from analysis if baseline bioluminescent signal was notably higher than the cohort or if mice had to be euthanized due to causes other than leukemia. NSG mice with baseline bioluminescent signals were randomly assigned into experimental groups. Anti-RSPO3 antibody was then administered at 20 mg/kg once weekly via i.p. injection. Imaging was thereafter performed once weekly. At the end of each experiment, BM cells were assessed by FACS analysis for leukemic cell engraftment and by confocal immunofluorescence and qPCR analysis for target expression.

For anti-RSPO3 treatment of newly-established PDX models, NSG mice were transplanted with primary AML patient samples harboring 9p deletion (7×10^6 cells per mouse), MLL-AF9 (1.6×10^6 cells per mouse) or MLL-AF1q (5.7×10^6 cells per mouse) followed directly by *in vivo* treatment with control versus anti-RSPO3 antibodies (20 mg/kg, i.p. every 4 days). Primary AML patient specimens harboring diagnosis or relapse MLL-AF10 (7.1×10^5 or 1.7×10^6 cells per mouse) did not engraft in NSG mice. Indicated numbers of transplanted patient cells were determined by their availability in our patient tumor bank and equal numbers of patient cells were transplanted into recipient mice. Mice were randomized into control versus treatment groups for each patient specimen. Researchers were not blinded to the treatment groups. BM cells were harvested for FACS analysis post-transplantation at time-points as indicated in the figure legends.

Leukemic cell stimulation with RSPO/WNT3 ligands

Wnt3 or control medium (Reya et al., 2003) was generated by sterile filtering the cultured medium of L-Wnt3 (CRL-2647) or L cells (CRL-2648) as described by the ATCC protocol. Recombinant mouse Rspo1 (3474-RS), Rspo2 (6946-RS), Rspo3 (4120-RS), Rspo4 (4106-RS), and recombinant human WNT3 (RDS5036WN010) were purchased from In Vitro Technologies. Recombinant human RSPO2 (120-43-20) and RSPO3 (120-44-20) were obtained from Lonza (Mount Waverley, VIC, Australia). For Western blot analysis of murine cells, 5×10^5 pre-LSCs were seeded in 24-well plates with IMDM media supplemented with Wnt3 (or control) medium and/or Rspo with indicated concentrations as well as mIL3, and incubated at 37°C for 24 h. For Western blot and immunofluorescence analysis of human AML cell lines, $3-5 \times 10^5$ leukemic cells were plated in a 6-well plate with 2 mL RPMI-1640 medium per well in the presence of 200 ng/mL of human WNT3 and/or RSPO2, as well as 1 μ M I-CBP112 (Sigma-Aldrich; 1134), and incubated at 37°C for the indicated times.

Viral vector production, cell transduction and bone marrow transplantation

MSCV-MLLAF9-GFP, MSCV-HOXA9-GFP, MSCV-MEIS1-puro and MSCV- β -catenin (β -cat*)-neo have been previously described (Krivtsov et al., 2006; Wang et al., 2010). MSCV-Lgr4-neo and LeGO-iT2-LGR4 vectors were generated by GenScript (NJ, USA). LeGO-iT2 was a gift from Boris Fehse (Addgene plasmid, 27343) (Weber et al., 2008). GNAS-pLX307 was a gift from William Hahn and Sefi Rosenbluh (Addgene plasmid, 98339) (Rosenbluh et al., 2016). Stable knockdown/knockout were achieved by using mouse Lgr4 shRNA sequences (Lgr4sh1: MSH040504-3-LVRU6MP; Lgr4sh2: MSH040504-4-LVRU6MP; scrambled control: CSHCTR001-LVRU6MP; GeneCopoeia, Rockville, MD, USA), human LGR4 shRNA sequences (LGR4sh1: TRCN0000273532; LGR4sh2: TRCN0000285015; scrambled control: SHC216; Sigma-Aldrich, Castle Hill, NSW, Australia) and lentiviral CRISPR/Cas9 plasmids (human LGR4 gRNA: HS0000422096; non-targeting control: CRISPR12, Sigma-Aldrich).

Viruses were produced by transfecting HEK293T with standard packaging vectors using lipofectamine 2000 (Life Technologies, Mulgrave, VIC, Australia) for murine AML cells and using lipofectamine 3000 (Life Technologies) for human leukemic cells. Viral supernatants were harvested 48-72 h following transfection, filtered through a 0.45- μm membrane and then concentrated by centrifugation. $1-5 \times 10^4$ cells were incubated with concentrated virus supplemented with 8 $\mu\text{g}/\text{mL}$ polybrene (Sigma-Aldrich). Four-hour transduction was performed for human PDX cells, overnight transduction for human leukemic cell lines and two rounds of transduction for murine leukemic cells. For BM transplantation, pre-LSCs or GFP⁺ leukemic cells flow-sorted from BM of AML mice were transplanted into sublethally irradiated (6 Gy) syngeneic BL6 recipient mice through intravenous (i.v.) injection.

Colony formation and serial replating assay

LSCs (Lin⁻Sca-1⁻c-Kit^{high}CD16/32^{high}CD34⁺), also known as L-GMP or GMP-like LSCs (Krivtsov et al., 2006), which were flow-sorted from the BM of AML mice, or pre-LSCs were seeded at a density of 1×10^3 cells per 35 mm dish in methylcellulose supplemented with mIL-3. Colonies were counted after 5 days of incubation at 37°C. For the serial replating assay, colonies were harvested and 1×10^3 cells were subsequently replated in fresh methylcellulose. Three rounds of serial replating were performed for each experiment.

***In vivo* bromodeoxyuridine (BrdU) cell proliferation assay**

GFP⁺ origin-specific leukemic BM cells from primary AML were transplanted into sublethally irradiated BL6 recipient mice for *in vivo* BrdU assays at 10 days post-transplantation. *In vivo* BrdU labeling was done by intraperitoneal (i.p.) injection of allophycocyanin (APC)-conjugated BrdU (1 mg/100 μl in PBS per mouse; BD Biosciences, 552598) for 2 h prior to bone marrow harvest following the manufacturer's protocol.

Cell cycle analysis

Cells were fixed in ice-cold 70% ethanol for 2 h at -20°C, stained with Alexa Fluor 647 mouse anti- Ki67 (BD Biosciences; 558615) and 7-amino-actinomycin D (7AAD, BD Biosciences) staining solution for 30 min at room temperature and analyzed by FACS analysis.

ROS production

ROS levels were detected by labeling 5×10^5 LSCs for 30 min at 37°C with 2.5 μM MitoSOXTM Red (Life Technologies) in PBS. Labeled cells were washed with PBS and analyzed by FACS.

The cAMP-Glo assay

The assay is based on the principle that G α_s -coupled receptors can promote direct activation of adenylyl cyclase leading to increased levels of cAMP, which in turn binds to and activates the exogenously added

PKA causing changes in ATP concentration and light production for luminescence measurements. 7×10^3 leukemic cells were plated in a 384-well plate in serum-free RPMI-1640 supplemented with IBMX and Imidazoline (Sigma-Aldrich) in the presence of 200 ng/mL of human WNT3 and/or RSPO2, and incubated at 37°C for 5 h. The cAMP-Glo Assay (Promega Corporation, Alexandria, NSW, Australia; V1501) was performed according to the manufacturer's instructions. The luciferase activity was measured with a luminometer (Victor3 plate reader; PerkinElmer, Waltham, MA, USA).

Western blot analysis

Western blots were performed according to standard laboratory protocols, using antibodies directed against LGR4 (Abcam; ab75501), phospho-Ser133-CREB (p-CREB^{Ser133}, Merck; 06-519), CREB (Sapphire Bioscience, Redfern, NSW, Australia; 3360R), β -catenin (BD Biosciences; 610154), active β -catenin (non-phospho-Ser33/Ser37/Thr41; Genesearch, Arundel, QLD, Australia; 8814), V5-Tag (Genesearch; 13202), H3K79me2 (Abcam; ab3594), total H3 (Abcam; ab1791), GAPDH (Abcam; ab8245) or ACTIN (Sigma-Aldrich; A2066). Blots were visualized and quantified using the ChemiDoc MP Imaging System (Bio-Rad) and the ImageJ software (Schneider et al., 2012). Relative protein band intensity was normalized against loading control (ACTIN, GAPDH or H3) and compared to relative control.

Confocal immunofluorescence

4×10^4 cells were cytopun onto glass slides, fixed in 4% paraformaldehyde in PBS for 10 min at room temperature and then washed three times for 5 min in PBS with 0.1% Tween-20 (PBS-T). Non-specific antibody binding was blocked with blocking media (10% goat serum and 2% BSA in PBS-T) for 1 h. Slides were stained overnight at 4°C with a primary antibody (i.e., active β -catenin, p-CREB^{Ser133}; CBP, MetaGene, Brisbane, QLD, Australia, sc-7300) at a dilution of 1:100, washed three times for 5 min in PBS-T, and then stained for 1 h with Alexa Fluor 568- or Alexa Fluor 647-conjugated secondary antibody (Abcam; ab175472 and ab150079), followed by staining with DAPI (1:4000, Thermo Fisher Scientific) for 30 min. Coverslips were mounted with ProLong Gold antifade mountant (Thermo Fisher Scientific) and edges were sealed with nail polish to prevent desiccation. Immunofluorescence images were taken with a TCS SP5 MP-STED confocal microscope (Leica Microsystems, Mannheim, Germany) and processed using NIH ImageJ software.

Quantitative real-time PCR (qPCR)

Total RNA was extracted from cells using the RNeasy Mini kit (Qiagen, Chadstone Centre, VIC, Australia). cDNA was synthesized from total RNA using oligo (dT) and M-MLV Reverse Transcriptase (Life Technologies). qPCR was performed using Power SYBR Green PCR Master Mix (Life Technologies) or SsoAdvanced Universal SYBR Green Supermix (Bio-Rad, Gladeville, NSW, Australia).

Target gene expression values were normalized against the house-keeping gene GAPDH.

QUANTIFICATION AND STATISTICAL ANALYSIS

Statistics

Statistical significance was determined by two-tailed unpaired Student's t-test to compare two groups of samples, one-way ANOVA and Dunnett test for multiple comparisons, and two-way ANOVA and Bonferroni correction for comparisons among groups with different time points. Kaplan-Meier plot and log-rank (Mantel-Cox) test were used to assess survival curves. Correlation analysis was performed by calculating the Pearson correlation coefficient. Throughout the manuscript, the following notation was used to indicate statistical significance: * $p < 0.05$, ** $p < 0.005$, *** $p < 0.0005$, **** $p < 0.0001$. Statistical parameters including the exact values of n and precision measure (mean \pm SD) and statistical significance are reported in the figures and figure legends. Statistical analysis and graph construction were performed using GraphPad Prism v7.04 (GraphPad Software, La Jolla, CA, USA).

Pearson correlation analysis of microarray data for AML patients

Affymetrix U133 Plus2.0 (HG133P2) array data has previously been published for patients in the USA cohort (Cancer Genome Atlas Research Network, 2013) and is available via the National Cancer Institute's Genomic Data Commons Portal (<https://portal.gdc.cancer.gov>). Matched clinical annotations and expression data was available for 183 AML patient samples including 47 classified into the adverse molecular risk group and 40 assigned into the European Leukemia Net adverse risk group (Dohner et al., 2010; Beck et al., 2018). The raw expression files of all 183 patient samples were processed using Partek Genomics Suite software v6.6 (Partek Inc., St. Louis, MO, USA) and normalized expression levels were generated after pre-processed including background subtractions, quantile normalization and log₂ transformation. The ComBat algorithm (Johnson et al., 2007) was used to remove experimental variation associated with different array batches. The Pearson correlation coefficient was calculated using GraphPad Prism between the expression level of the probesets representing *LGR4* and *HOXA9*. The significance level of this correlation was tested using a t-distribution, to assess whether the correlation differed significantly from zero (threshold of $p < 0.05$).

Genome-wide profiling analysis

Microarray data, including GSE29828 (Daigle et al., 2011) and GSE13714 (Faber et al., 2009), were analyzed using the GenePattern software (Reich et al., 2006) as previously described (Wang et al., 2010). ChIP-seq data, including GSM1519628 and GSE43063 (Chen et al., 2015; Deshpande et al., 2013), were visualized with the Integrative Genomics Viewer (IGV) software (Thorvaldsdottir et al., 2013).

REFERENCES

- Abramovich, C., and Humphries, R. K. (2005). Hox regulation of normal and leukemic hematopoietic stem cells. *Curr Opin Hematol* 12, 210-216.
- Akashi, K., Traver, D., Miyamoto, T., and Weissman, I. L. (2000). A clonogenic common myeloid progenitor that gives rise to all myeloid lineages. *Nature* 404, 193-197.
- Bagger, F. O., Sasivarevic, D., Sohi, S. H., Laursen, L. G., Pundhir, S., Sonderby, C. K., Winther, O., Rapin, N., and Porse, B. T. (2016). BloodSpot: a database of gene expression profiles and transcriptional programs for healthy and malignant haematopoiesis. *Nucleic Acids Res* 44, D917-924.
- Beck, D., Thoms, J.A.I., Palu, C., Herold, T., Shah, A., Olivier, J., Boelen, L., Huang, Y., Chacon, D., Brown, A., *et al.* (2018). A four-gene LincRNA expression signature predicts risk in multiple cohorts of acute myeloid leukemia patients. *Leukemia* 32, 263-272.
- Bendell, J., Eckhardt, G. S., Hochster, H. S., Morris, V. K., Strickler, J., Kapoun, A. M., Wang, M., Xu, L., McGuire, K., Dupont, J., *et al.* (2016). Initial results from a phase 1a/b study of OMP-131R10, a first-in-class anti-RSPO3 antibody, in advanced solid tumors and previously treated metastatic colorectal cancer (CRC). *European Journal of Cancer* 69, S29-S30.
- Bernt, K. M., Zhu, N., Sinha, A. U., Vempati, S., Faber, J., Krivtsov, A. V., Feng, Z., Punt, N., Daigle, A., Bullinger, L., *et al.* (2011). MLL-rearranged leukemia is dependent on aberrant H3K79 methylation by DOT1L. *Cancer cell* 20, 66-78.
- Calvo, K. R., Knoepfler, P. S., Sykes, D. B., Pasillas, M. P., and Kamps, M. P. (2001). Meis1a suppresses differentiation by G-CSF and promotes proliferation by SCF: potential mechanisms of cooperativity with Hoxa9 in myeloid leukemia. *Proceedings of the National Academy of Sciences of the United States of America* 98, 13120-13125.
- Cancer Genome Atlas Research, N. (2013). Genomic and epigenomic landscapes of adult de novo acute myeloid leukemia. *The New England journal of medicine* 368, 2059-2074.
- Carmon, K. S., Gong, X., Lin, Q., Thomas, A., and Liu, Q. (2011). R-spondins function as ligands of the orphan receptors LGR4 and LGR5 to regulate Wnt/beta-catenin signaling. *Proceedings of the National Academy of Sciences of the United States of America* 108, 11452-11457.
- Chartier, C., Raval, J., Axelrod, F., Bond, C., Cain, J., Dee-Hoskins, C., Ma, S., Fischer, M. M., Shah, J., Wei, J., *et al.* (2016). Therapeutic targeting of tumor-derived R-Spondin attenuates β -catenin signaling and tumorigenesis in multiple cancer types. *Cancer research* 76, 713-723.
- Chen, C. W., Koche, R. P., Sinha, A. U., Deshpande, A. J., Zhu, N., Eng, R., Doench, J. G., Xu, H., Chu, S. H., Qi, J., *et al.* (2015). DOT1L inhibits SIRT1-mediated epigenetic silencing to maintain leukemic gene expression in MLL-rearranged leukemia. *Nat Med* 21, 335-343.
- Chen, L., Deshpande, A. J., Banka, D., Bernt, K. M., Dias, S., Buske, C., Olhava, E. J., Daigle, S. R., Richon, V. M., Pollock, R. M., and Armstrong, S. A. (2013). Abrogation of MLL-AF10 and CALM-AF10-mediated transformation through genetic inactivation or pharmacological inhibition of the H3K79 methyltransferase Dot1l. *Leukemia* 27, 813-822.
- Chrivia, J. C., Kwok, R. P., Lamb, N., Hagiwara, M., Montminy, M. R., and Goodman, R. H. (1993). Phosphorylated CREB binds specifically to the nuclear protein CBP. *Nature* 365, 855-859.
- Clevers, H., and Nusse, R. (2012). Wnt/beta-catenin signaling and disease. *Cell* 149, 1192-1205.
- Cozzio, A., Passegue, E., Ayton, P. M., Karsunky, H., Cleary, M. L., and Weissman, I. L. (2003). Similar MLL-associated leukemias arising from self-renewing stem cells and short-lived myeloid progenitors. *Genes & development* 17, 3029-3035.
- Daigle, S. R., Olhava, E. J., Therkelsen, C. A., Majer, C. R., Sneeringer, C. J., Song, J., Johnston, L. D., Scott, M. P., Smith, J. J., Xiao, Y., *et al.* (2011). Selective killing of mixed lineage leukemia cells by a potent small-molecule DOT1L inhibitor. *Cancer cell* 20, 53-65.
- de Lau, W., Barker, N., Low, T. Y., Koo, B. K., Li, V. S., Teunissen, H., Kujala, P., Haegbarth, A., Peters, P. J., van de Wetering, M., *et al.* (2011). Lgr5 homologues associate with Wnt receptors and mediate R-spondin signalling. *Nature* 476, 293-297.
- Deshpande, A. J., Chen, L., Fazio, M., Sinha, A. U., Bernt, K. M., Banka, D., Dias, S., Chang, J., Olhava,

E. J., Daigle, S. R., *et al.* (2013). Leukemic transformation by the MLL-AF6 fusion oncogene requires the H3K79 methyltransferase Dot1l. *Blood* *121*, 2533-2541.

Dietrich, P. A., Yang, C., Leung, H. H., Lynch, J. R., Gonzales, E., Liu, B., Haber, M., Norris, M. D., Wang, J., and Wang, J. Y. (2014). GPR84 sustains aberrant beta-catenin signaling in leukemic stem cells for maintenance of MLL leukemogenesis. *Blood* *124*, 3284-3294.

Dohner, H., Estey, E. H., Amadori, S., Appelbaum, F. R., Buchner, T., Burnett, A. K., Dombret, H., Fenaux, P., Grimwade, D., Larson, R. A., *et al.* (2010). Diagnosis and management of acute myeloid leukemia in adults: recommendations from an international expert panel, on behalf of the European LeukemiaNet. *Blood* *115*, 453-474.

Faber, J., Krivtsov, A. V., Stubbs, M. C., Wright, R., Davis, T. N., van den Heuvel-Eibrink, M., Zwaan, C. M., Kung, A. L., and Armstrong, S. A. (2009). HOXA9 is required for survival in human MLL-rearranged acute leukemias. *Blood* *113*, 2375-2385.

Golub, T. R., Slonim, D. K., Tamayo, P., Huard, C., Gaasenbeek, M., Mesirov, J. P., Coller, H., Loh, M. L., Downing, J. R., Caligiuri, M. A., *et al.* (1999). Molecular classification of cancer: class discovery and class prediction by gene expression monitoring. *Science* *286*, 531-537.

Gonzales-Aloy, E., Connerty, P., Salik, B., Liu, B., Woo, A. J., Haber, M., Norris, M. D., Wang, J., and Wang, J. Y. (2019). miR-101 suppresses the development of MLL-rearranged acute myeloid leukemia. *Haematologica* *104*, e296-e299.

Hoffmeyer, K., Junghans, D., Kanzler, B., and Kemler, R. (2017). Trimethylation and acetylation of beta-catenin at lysine 49 represent key elements in ESC pluripotency. *Cell Rep* *18*, 2815-2824.

Hope, K. J., Jin, L., and Dick, J. E. (2004). Acute myeloid leukemia originates from a hierarchy of leukemic stem cell classes that differ in self-renewal capacity. *Nat Immunol* *5*, 738-743.

Johnson, W. E., Li, C., and Rabinovic, A. (2007). Adjusting batch effects in microarray expression data using empirical Bayes methods. *Biostatistics* *8*, 118-127.

Kawagoe, H., Humphries, R. K., Blair, A., Sutherland, H. J., and Hogge, D. E. (1999). Expression of HOX genes, HOX cofactors, and MLL in phenotypically and functionally defined subpopulations of leukemic and normal human hematopoietic cells. *Leukemia* *13*, 687-698.

Kazanskaya, O., Glinka, A., del Barco Barrantes, I., Stanek, P., Niehrs, C., and Wu, W. (2004). R-Spondin2 is a secreted activator of Wnt/beta-catenin signaling and is required for *Xenopus* myogenesis. *Developmental cell* *7*, 525-534.

Kazanskaya, O., Ohkawara, B., Heroult, M., Wu, W., Maltry, N., Augustin, H. G., and Niehrs, C. (2008). The Wnt signaling regulator R-spondin 3 promotes angioblast and vascular development. *Development* *135*, 3655-3664.

Kim, K. A., Kakitani, M., Zhao, J., Oshima, T., Tang, T., Binnerts, M., Liu, Y., Boyle, B., Park, E., Emtage, P., *et al.* (2005). Mitogenic influence of human R-spondin1 on the intestinal epithelium. *Science* *309*, 1256-1259.

Konopleva, M. Y., and Jordan, C. T. (2011). Leukemia stem cells and microenvironment: biology and therapeutic targeting. *J Clin Oncol* *29*, 591-599.

Krevvata, M., Shan, X., Zhou, C., Dos Santos, C., Habineza Ndikuyeze, G., Secreto, A., Glover, J., Trotman, W., Brake-Silla, G., Nunez-Cruz, S., *et al.* (2018). Cytokines increase engraftment of human acute myeloid leukemia cells in immunocompromised mice but not engraftment of human myelodysplastic syndrome cells. *Haematologica* *103*, 959-971.

Krivtsov, A. V., and Armstrong, S. A. (2007). MLL translocations, histone modifications and leukaemia stem-cell development. *Nat Rev Cancer* *7*, 823-833.

Krivtsov, A. V., Figueroa, M. E., Sinha, A. U., Stubbs, M. C., Feng, Z., Valk, P. J., Delwel, R., Dohner, K., Bullinger, L., Kung, A. L., *et al.* (2013). Cell of origin determines clinically relevant subtypes of MLL-rearranged AML. *Leukemia* *27*, 852-860.

Krivtsov, A. V., Twomey, D., Feng, Z., Stubbs, M. C., Wang, Y., Faber, J., Levine, J. E., Wang, J., Hahn, W. C., Gilliland, D. G., *et al.* (2006). Transformation from committed progenitor to leukaemia stem cell

initiated by MLL-AF9. *Nature* 442, 818-822.

Kroon, E., Kros, J., Thorsteinsdottir, U., Baban, S., Buchberg, A. M., and Sauvageau, G. (1998). Hoxa9 transforms primary bone marrow cells through specific collaboration with Meis1a but not Pbx1b. *EMBO J* 17, 3714-3725.

Lawrence, H. J., Rozenfeld, S., Cruz, C., Matsukuma, K., Kwong, A., Komuves, L., Buchberg, A. M., and Largman, C. (1999). Frequent co-expression of the HOXA9 and MEIS1 homeobox genes in human myeloid leukemias. *Leukemia* 13, 1993-1999.

Liu, D., He, X. C., Qian, P., Barker, N., Trainor, P. A., Clevers, H., Liu, H., and Li, L. (2014). Leucine-rich repeat-containing G-protein-coupled Receptor 5 marks short-term hematopoietic stem and progenitor cells during mouse embryonic development. *The Journal of biological chemistry* 289, 23809- 23816.

Luis, T. C., Weerkamp, F., Naber, B. A., Baert, M. R., de Haas, E. F., Nikolic, T., Heuvelmans, S., De Krijger, R. R., van Dongen, J. J., and Staal, F. J. (2009). Wnt3a deficiency irreversibly impairs hematopoietic stem cell self-renewal and leads to defects in progenitor cell differentiation. *Blood* 113, 546-554.

Luo, J., Yang, Z., Ma, Y., Yue, Z., Lin, H., Qu, G., Huang, J., Dai, W., Li, C., Zheng, C., *et al.* (2016). LGR4 is a receptor for RANKL and negatively regulates osteoclast differentiation and bone resorption. *Nat Med* 22, 539-546.

Lynch, J. R., Salik, B., Connerty, P., Vick, B., Leung, H., Pijning, A., Jeremias, I., Spiekermann, K., Trahair, T., Liu, T., *et al.* (2019). JMJD1C-mediated metabolic dysregulation contributes to HOXA9-dependent leukemogenesis. *Leukemia* 33, 1400-1410.

Lynch, J. R., and Wang, J. Y. (2016). G Protein-Coupled Receptor Signaling in Stem Cells and Cancer. *Int J Mol Sci* 17.

Lynch, J. R., Yi, H., Casolari, D. A., Voli, F., Gonzales-Aloy, E., Fung, T. K., Liu, B., Brown, A., Liu, T., Haber, M., *et al.* (2016). Gαq signaling is required for the maintenance of MLL-AF9-induced acute myeloid leukemia. *Leukemia* 30, 1745-1748.

Majeti, R., Becker, M. W., Tian, Q., Lee, T. L., Yan, X., Liu, R., Chiang, J. H., Hood, L., Clarke, M. F., and Weissman, I. L. (2009). Dysregulated gene expression networks in human acute myelogenous leukemia stem cells. *Proc Natl Acad Sci U S A* 106, 3396-3401.

Mazerbourg, S., Bouley, D. M., Sudo, S., Klein, C. A., Zhang, J. V., Kawamura, K., Goodrich, L. V., Rayburn, H., Tessier-Lavigne, M., and Hsueh, A. J. (2004). Leucine-rich repeat-containing, G protein-coupled receptor 4 null mice exhibit intrauterine growth retardation associated with embryonic and perinatal lethality. *Mol Endocrinol* 18, 2241-2254.

Metzeler, K. H., Herold, T., Rothenberg-Thurley, M., Amler, S., Sauerland, M. C., Gorlich, D., Schneider, S., Konstandin, N. P., Dufour, A., Braundl, K., *et al.* (2016). Spectrum and prognostic relevance of driver gene mutations in acute myeloid leukemia. *Blood* 128, 686-698.

Muntean, A. G., and Hess, J. L. (2012). The pathogenesis of mixed-lineage leukemia. *Annu Rev Pathol* 7, 283-301.

Reich, M., Liefeld, T., Gould, J., Lerner, J., Tamayo, P., and Mesirov, J. P. (2006). GenePattern 2.0. *Nat Genet* 38, 500-501.

Reya, T., Duncan, A. W., Ailles, L., Domen, J., Scherer, D. C., Willert, K., Hintz, L., Nusse, R., and Weissman, I. L. (2003). A role for Wnt signalling in self-renewal of haematopoietic stem cells. *Nature* 423, 409-414.

Rosenbluh, J., Mercer, J., Shrestha, Y., Oliver, R., Tamayo, P., Doench, John G., Tirosh, I., Piccioni, F., Hartenian, E., Horn, H., *et al.* (2016). Genetic and proteomic interrogation of lower confidence candidate genes reveals signaling networks in β-catenin-active cancers. *Cell Systems* 3, 302-316.e304.

Schneider, C. A., Rasband, W. S., and Eliceiri, K. W. (2012). NIH Image to ImageJ: 25 years of image analysis. *Nat Methods* 9, 671-675.

Shankar, D. B., Cheng, J. C., Kinjo, K., Federman, N., Moore, T. B., Gill, A., Rao, N. P., Landaw, E. M., and Sakamoto, K. M. (2005). The role of CREB as a proto-oncogene in hematopoiesis and in acute myeloid leukemia. *Cancer cell* 7, 351-362.

Simon, M., Grandage, V. L., Linch, D. C., and Khwaja, A. (2005). Constitutive activation of the Wnt/beta-catenin signalling pathway in acute myeloid leukaemia. *Oncogene* *24*, 2410-2420.

Stavropoulou, V., Kaspar, S., Brault, L., Sanders, M. A., Juge, S., Morettini, S., Tzankov, A., Iacovino, M., Lau, I. J., Milne, T. A., *et al.* (2016). MLL-AF9 Expression in Hematopoietic Stem Cells Drives a Highly Invasive AML Expressing EMT-Related Genes Linked to Poor Outcome. *Cancer cell* *30*, 43- 58.

Tamai, K., Semenov, M., Kato, Y., Spokony, R., Liu, C., Katsuyama, Y., Hess, F., Saint-Jeannet, J.-P., and He, X. (2000). LDL-receptor-related proteins in Wnt signal transduction. *Nature* *407*, 530.

Thorvaldsdottir, H., Robinson, J. T., and Mesirov, J. P. (2013). Integrative Genomics Viewer (IGV): high-performance genomics data visualization and exploration. *Brief Bioinform* *14*, 178-192.

Vick, B., Rothenberg, M., Sandhofer, N., Carlet, M., Finkenzeller, C., Krupka, C., Grunert, M., Trumpp, A., Corbacioglu, S., Ebinger, M., *et al.* (2015). An advanced preclinical mouse model for acute myeloid leukemia using patients' cells of various genetic subgroups and in vivo bioluminescence imaging. *PLoS One* *10*, e0120925.

Wang, Y., Krivtsov, A. V., Sinha, A. U., North, T. E., Goessling, W., Feng, Z., Zon, L. I., and Armstrong, S. A. (2010). The Wnt/beta-catenin pathway is required for the development of leukemia stem cells in AML. *Science* *327*, 1650-1653.

Weber, K., Bartsch, U., Stocking, C., and Fehse, B. (2008). A multicolor panel of novel lentiviral "gene ontology" (LeGO) vectors for functional gene analysis. *Mol Ther* *16*, 698-706.

Welch, J. S., Ley, T. J., Link, D. C., Miller, C. A., Larson, D. E., Koboldt, D. C., Wartman, L. D., Lamprecht, T. L., Liu, F., Xia, J., *et al.* (2012). The origin and evolution of mutations in acute myeloid leukemia. *Cell* *150*, 264-278.

Willert, K., Brown, J. D., Danenberg, E., Duncan, A. W., Weissman, I. L., Reya, T., Yates, J. R., 3rd, and Nusse, R. (2003). Wnt proteins are lipid-modified and can act as stem cell growth factors. *Nature* *423*, 448-452.

Yeung, J., Esposito, M. T., Gandillet, A., Zeisig, B. B., Griessinger, E., Bonnet, D., and So, C. W. (2010). beta-catenin mediates the establishment and drug resistance of MLL leukemic stem cells. *Cancer cell* *18*, 606-618.

Ysebaert, L., Chicanne, G., Demur, C., De Toni, F., Prade-Houdellier, N., Ruidavets, J. B., Mansat-De Mas, V., Rigal-Huguet, F., Laurent, G., Payrastre, B., *et al.* (2006). Expression of beta-catenin by acute myeloid leukemia cells predicts enhanced clonogenic capacities and poor prognosis. *Leukemia* *20*, 1211-1216.

KEY RESOURCES TABLE

REAGENT or RESOURCE	SOURCE	IDENTIFIER
Antibodies		
Rabbit polyclonal anti-phospho-CREB (Ser133)	Merck	Cat# 06-519; RRID: AB_310153
Rabbit polyclonal anti-CREB	Sapphire Bioscience	Cat# 3360R; RRID: AB_2292322
Rabbit polyclonal anti-LGR4	Abcam	Cat# ab75501; RRID: AB_1523714
Rabbit polyclonal anti-LGR4 for flow cytometry	Abcam	Cat# ab137480
Mouse monoclonal anti- β -catenin	BD Bioscience	Cat# 610154; RRID: AB_397555
Rabbit monoclonal anti- β -catenin (non-phospho-Ser33/Ser37/Thr41)	Genesearch	Cat# 8814; RRID: AB_11127203
Rabbit monoclonal anti-V5-Tag	Genesearch	Cat# 13202; RRID: AB_2687461
Rabbit polyclonal anti-H3K79me2 - ChIP Grade	Abcam	Cat# ab3594; RRID: AB_303937
Rabbit polyclonal anti-H3 - ChIP Grade	Abcam	Cat# ab1791; RRID: AB_302613
Mouse monoclonal anti-GAPDH	Abcam	Cat# ab8245; RRID: AB_2107448
Rabbit polyclonal anti-Actin	Sigma-Aldrich	Cat# A2066; RRID: AB_476693
Donkey anti-mouse Alexa Fluor 568	Abcam	Cat# ab175472; RRID: AB_2636996
Goat anti-Rabbit Alexa Fluor 647	Abcam	Cat# ab150079; RRID: AB_2722623
Mouse monoclonal Ki-67 antibody	BD Bioscience	Cat# 558615; RRID: AB_647130
Alexa Fluor 647 anti-human CD34	BioLegend	Cat# 343508; RRID: AB_1877133
PE anti-human CD33	BioLegend	Cat# 303404; RRID: AB_314348
APC anti-human CD45	BD Bioscience	Cat# 555485; RRID: AB_398600
FITC anti-human CD45	BD Bioscience	Cat# 347463; RRID: AB_400306
FITC anti-mouse CD45	BD Bioscience	Cat#553080; RRID: AB_394610
Bacterial and Virus Strains		
See Table S3		
Biological Samples		

Human: primary AML patient specimens carrying MLL- AF9, MLL-AF10, MLL-AF1q, AML1-ETO, 9p deletion or with normal karyotype	This study	N/A
Patient-derived xenograft (PDX)	Vick et al., 2015	N/A
Human: primary CD34 ⁺ HSPCs	Lonza	Cat# 2M-101C
Chemicals, Peptides, and Recombinant Proteins		
Clinical-stage anti-RSPO3 monoclonal antibody	OncoMed Pharmaceuticals	OMP-131R10
I-CBP112 (selective CBP/p300 BRD inhibitor)	Sigma-Aldrich	Cat# 1134; CAS: 1640282-31-0
Human RSPO2	Lonza	Cat# 120-43-20
Human RSPO3	Lonza	Cat# 120-44-20
Human WNT3	In Vitro Technologies	RDS5036WN010
StemSpan™ CD34 ⁺ Expansion Supplement [x10] consisting of human SCF, FLT3-L, TPO, IL-3 and IL-6	StemCell Technologies	Cat# 02691
Mouse Rspo1	In Vitro Technologies	Cat# 3474-RS
Mouse Rspo2	In Vitro Technologies	Cat# 6946-RS
Mouse Rspo3	In Vitro Technologies	Cat# 4120-RS
Mouse Rspo4	In Vitro Technologies	Cat# 4106-RS
Mouse Wnt3	ATCC	L-Wnt3 (Wnt3): Cat# CRL-2647 L cells (control): Cat# CRL-2648
Mouse IL-3	StemCell Technologies	Cat# 78042
Critical Commercial Assays		
EasySep™ human CD34 positive selection Kit	StemCell Technologies	Cat# 18056
EasySep™ human CD33 positive selection Kit	StemCell Technologies	Cat# 18287
APC BrdU Flow Kit	BD Biosciences	Cat# 552598
cAMP-Glo assay	Promega Corporation	Cat# V1501
RNeasy Mini Kit	Qiagen	Cat# 74104
Deposited Data		
H3K79me2 ChIP-seq of human MOLM-13 & HL-60 cells	Deshpande et al., 2013	GEO: GSE43063
H3K79me2 ChIP-seq of human MOLM-13 cells	Chen et al., 2015	GEO: GSM1519628
Microarray of human MOLM-13 cells treated with DMSO versus EPZ004777 (DOT1L inhibitor)	Daigle et al., 2011	GEO: GSE29828
Microarray of human MOLM-14 cells transduced with control versus HOXA9 shRNA	Faber et al., 2009	GEO: GSE13714

Microarray of several cohorts of primary AML patients versus normal human HSCs	Bagger et al., 2016	GEO: AML patients: GSE13159, GSE15434, GSE61804, GSE14468, and The Cancer Genome Atlas TCGA; Normal human HSCs: GSE42519
Experimental Models: Cell Lines		
Human AML cell line (THP-1)	ATCC	TIB-202
Human acute promyelocytic leukemia cell line (HL-60)	ATCC	CCL-240
Human CML cell line (K562)	ATCC	CCL-243
Human AML cell line (MOLM-13)	DSMZ	ACC 554
Human embryonic kidney 293T cell line (HEK293T)	ATCC	CRL-11268
Experimental Models: Organisms/Strains		
Mouse: C57BL/6	Australian BioResources Mossvale	N/A
Mouse: NOD.Cg-Prkdc ^{scid} Il2rg ^{tm1Wjl} /SzJ (NSG)	Australian BioResources Mossvale	N/A
Mouse: Patient-derived xenograft (PDX)	Vick et al., 2015	N/A
Oligonucleotides		
Primers, see Table S4	This study	N/A
Software and Algorithms		
FlowJo Software	TreeStar	In house license
ImageJ	Schneider et al., 2012	https://imagej.nih.gov/ij/
GenePattern	Reich et al., 2006	http://software.broadinstitute.org/cancer/software/genepattern/
Integrative Genomics Viewer (IGV)	Thorvaldsdottir et al., 2013	https://software.broadinstitute.org/software/igv/
Living Image Software (v3.0)	Xenogen	In house license
GraphPad Prism 7	GraphPad Software	In house license
Partek Genomics Suite (v6.6)	Partek	In house license
FACS DIVA Software	BD	In house license

FIGURE 1

See also Figure S1

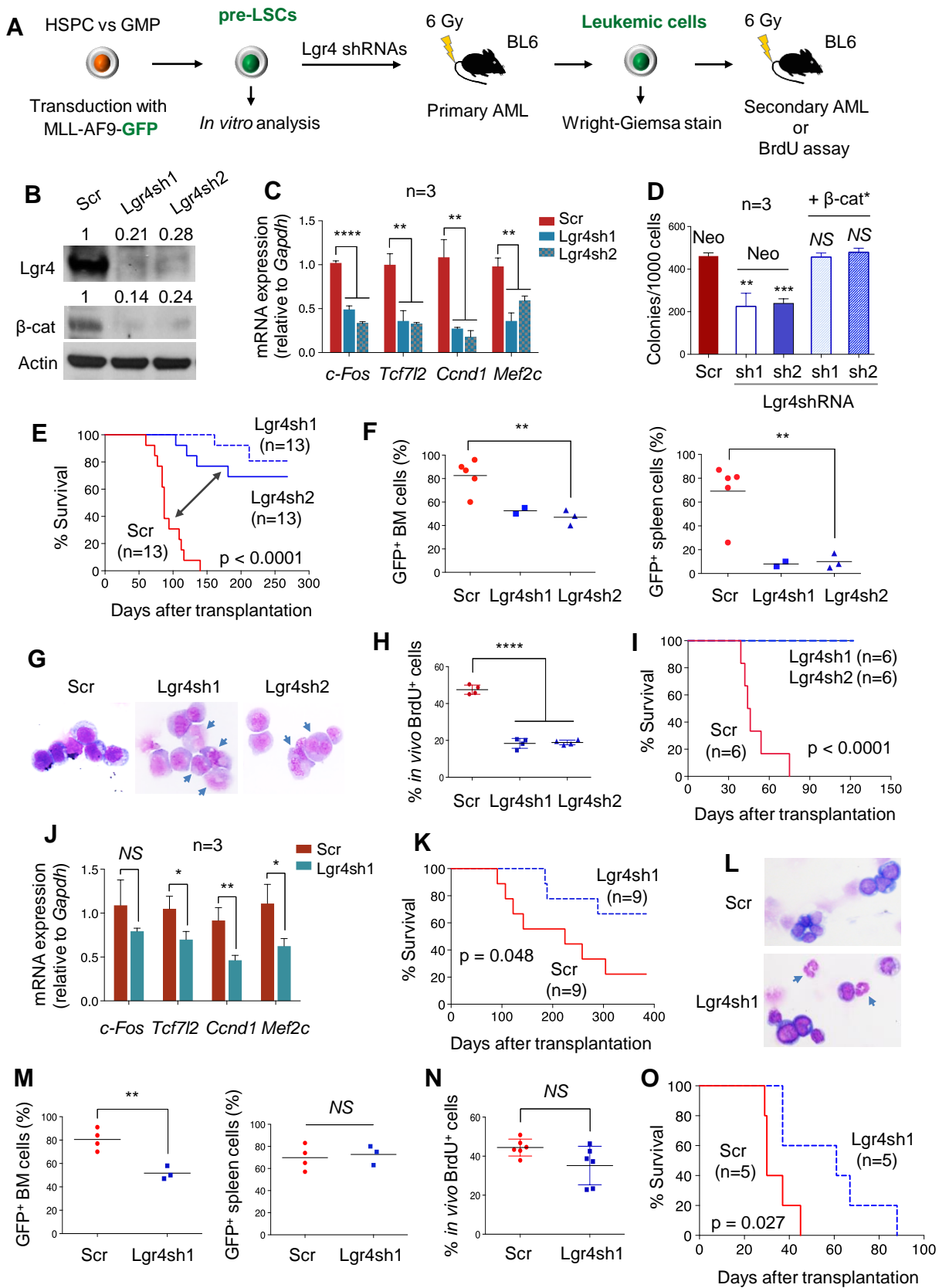


FIGURE 2

See also Figures S2-S3

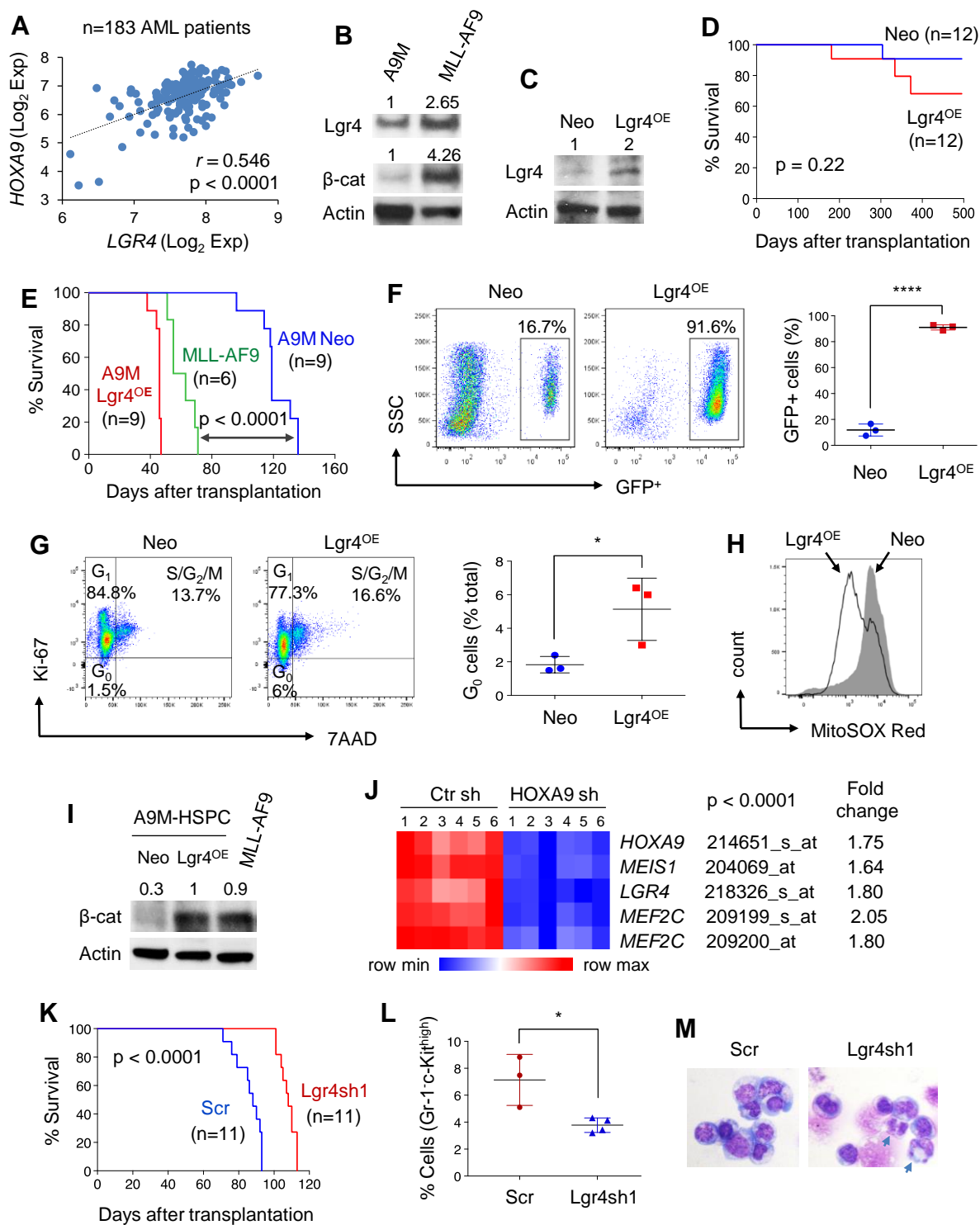


FIGURE 3

See also Figure S4 and Table S1

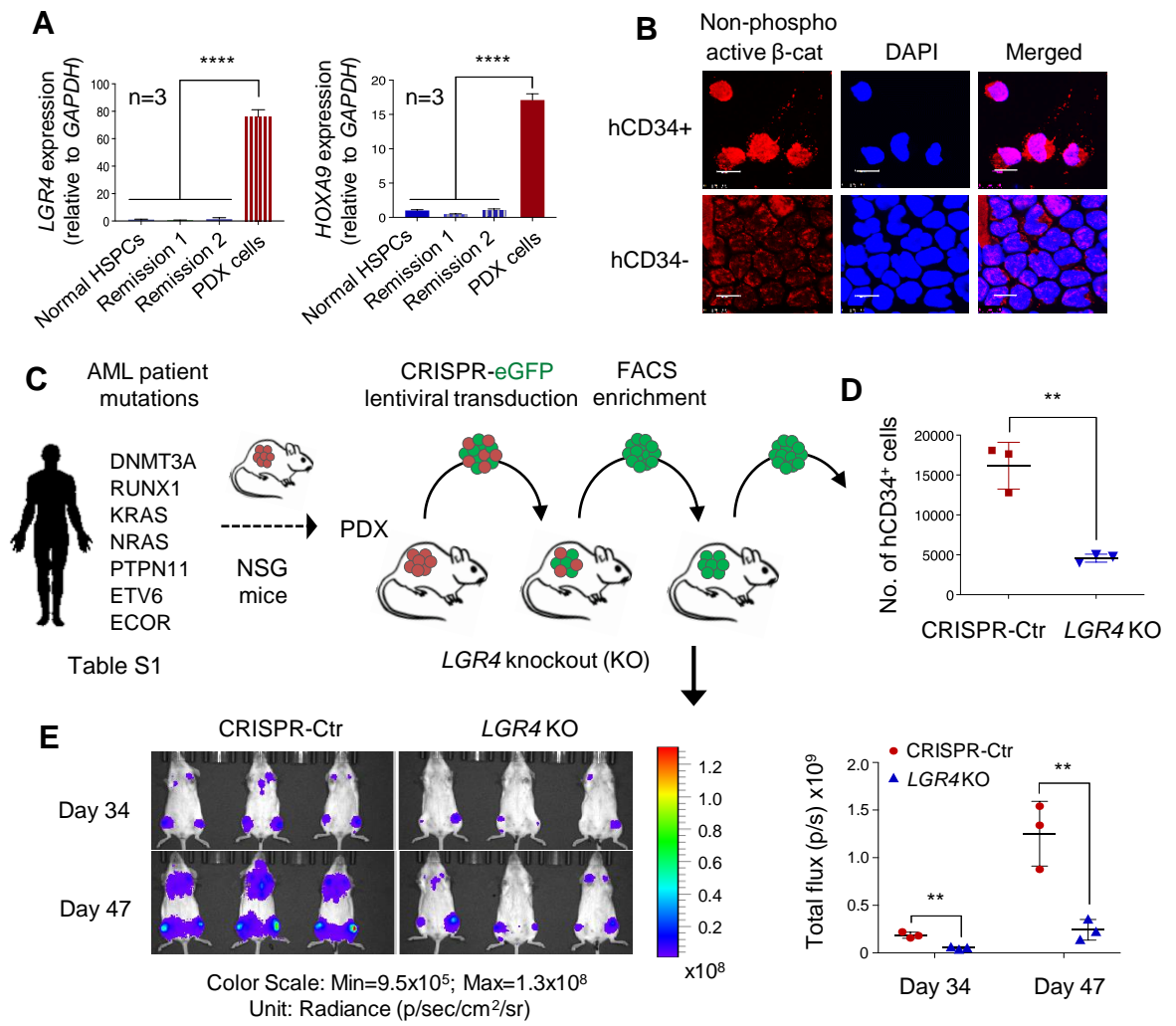


FIGURE 4

See also Figures S5-S6 and Table S2

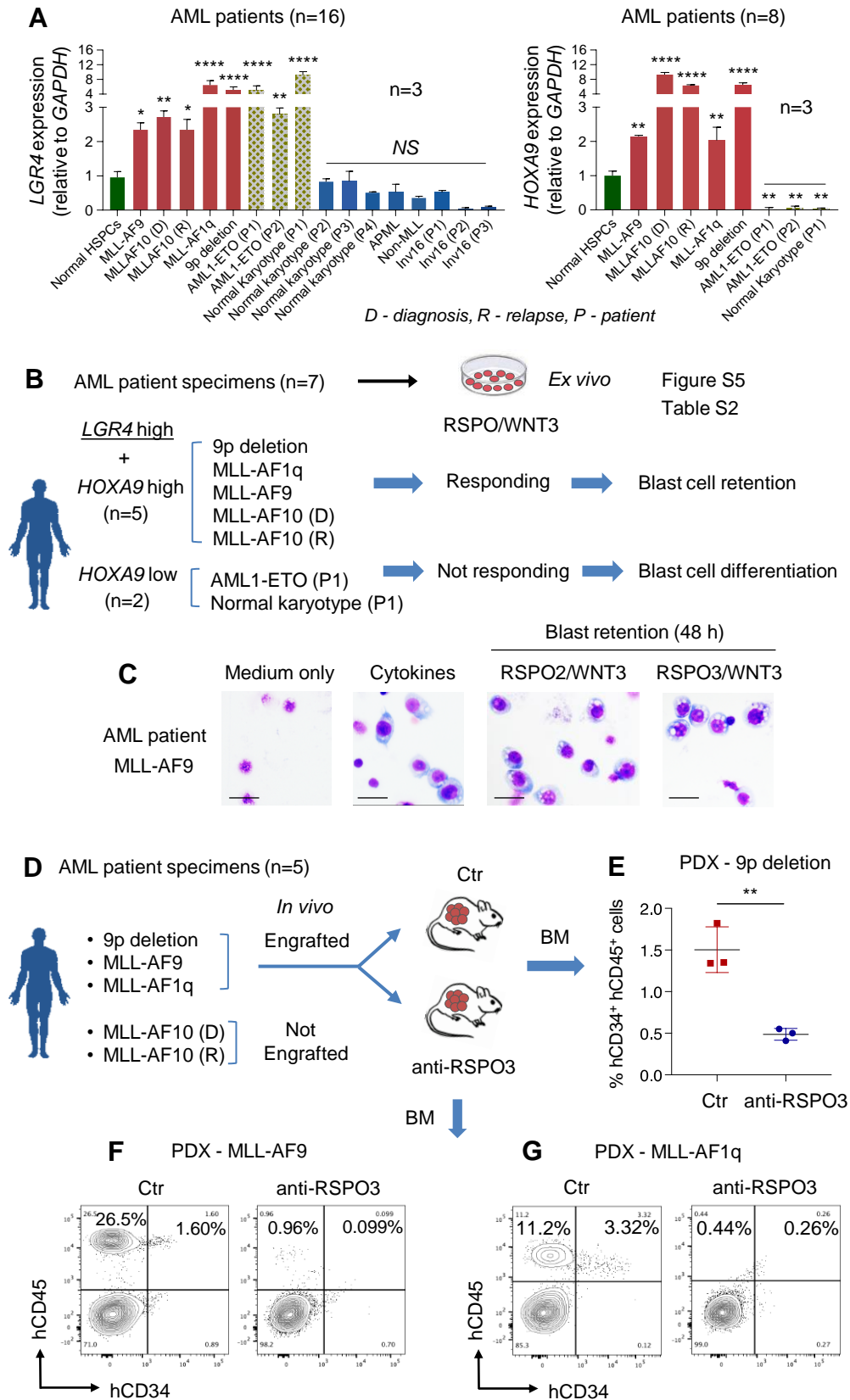


FIGURE 5

See also Figure S7

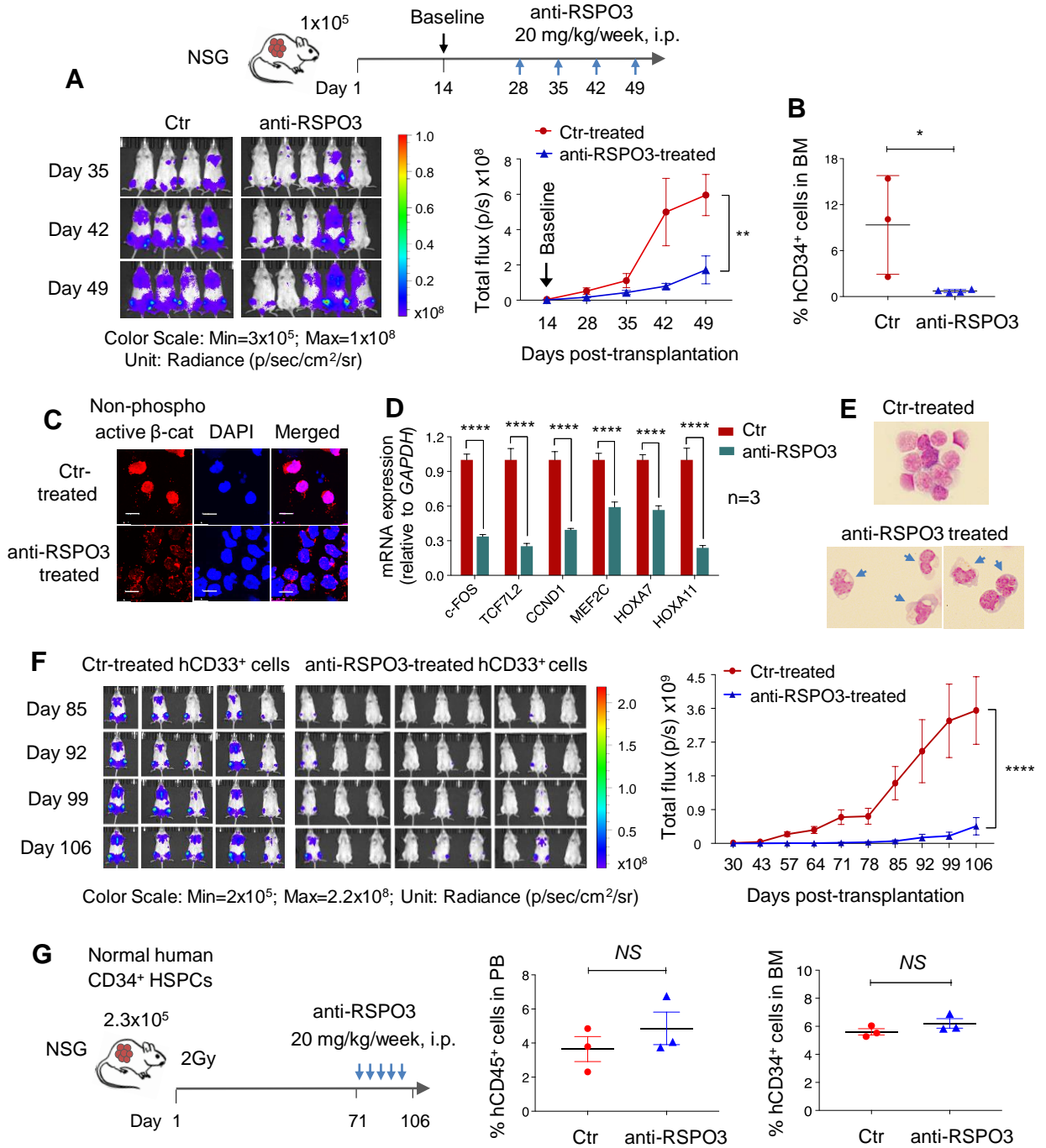


FIGURE 6

See also Figure S8

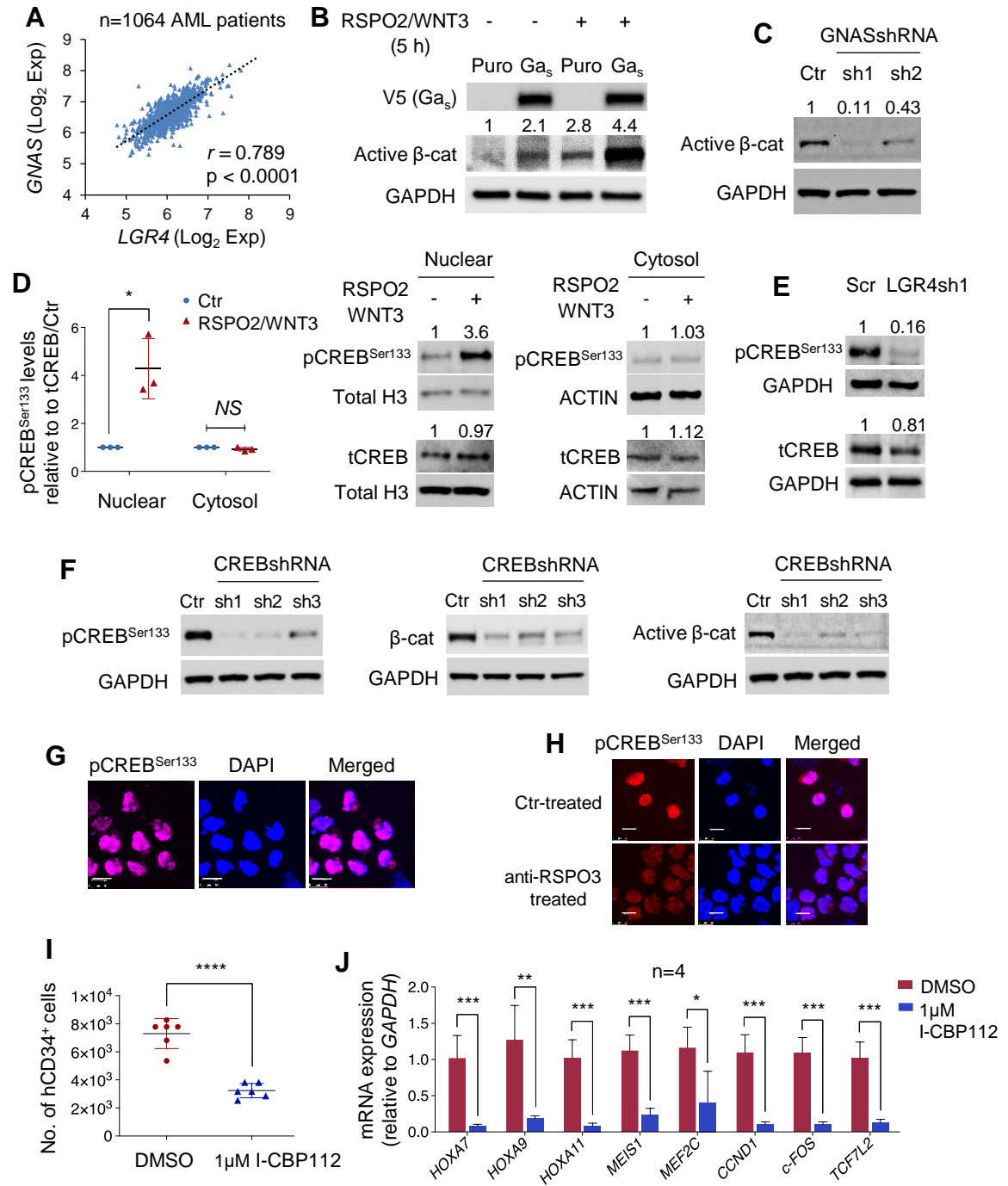


Table 1. Clinical characteristics of AML patient samples.

AML Diagnosis	Cytogenetics	Time point	% Blasts	FISH	Sex	Age (y) at diagnosis / relapse	Time from diagnosis (y)	Alive	Disease free	Cause of death
9p deletion	46,XX,add(9)(p11){6}/46XX{14}	Diagnosis	96	NA	Female	9.4	5.0	Yes	Yes	
MLL-AF9	47,XX,+8,t(9;11)(p22;q23)20	Diagnosis	80-90	nuc ish(KMT2Ax2)(5'KMT2A sep 3'KMT2Ax1)88/100	Female	16.7	1.8	Yes	Yes	
MLL-AF1q	46,XX,t(1;11)(q21;q23)[2]/48,XX,s1,+13,+19[18]	Diagnosis	90	NA	Female	1.5	13	Yes	Yes	
MLL-AF10	47,XX,der(10)inv(11)(q13q23)t(10;11)(p11.2;q11),der(11)t(10;11),+mar1[3]/48,s1,+mar1[17]	Relapse	71	nuc ish(KMT2Ax2)(5'KMT2A sep 3'KMT2Ax1)[108/125]	Female	17.2		No	No	Disease progression
MLL-AF10	46,XX,der(10)inv(11)(q13q23)t(10;11)(p11.2;q11),der(11)t(10;11)[20]	Diagnosis	84	nuc ish(KMT2Ax2)(3'KMT2A sep 5'KMT2Ax1)[140/150]	Female	16.0	1.3	No	No	Disease progression
Normal karyotype	46,XY	Diagnosis	55	NA	Male	14.2	11.3	Yes	Yes	
AML1-ETO	45,X,-Y,t(8;21)(q22;q22){20}	Diagnosis	34	t(8;21)	Male	9.5	11.7	Yes	Yes	

Table S3, related to STAR Methods. Viral plasmids used in this study.

Viral plasmids	SOURCE	IDENTIFIER
Lentiviral LeGO-iT2	A gift from Boris Fehse (Weber et al., 2008)	Addgene plasmid, #27343
Lentiviral LeGO-iT2-LGR4	This study	N/A
Retroviral MSCV-Lgr4-neo	This study	N/A
Lentiviral GNAS_pLX307	A gift from William Hahn and Sefi Rosenbluh (Rosenbluh et al., 2016)	Addgene plasmid, #98339
Retroviral MSCV-MLLAF9-GFP	Krivtsov et al., 2006	N/A
Retroviral MSCV-HOXA9-GFP	Wang et al., 2010	N/A
Retroviral MSCV-MEIS1-puro	Wang et al., 2010	N/A
Retroviral MSCV- β -catenin (β -cat*)-neo	Wang et al., 2010	N/A
Lentiviral mouse Lgr4 shRNA1	GeneCopoeia	MSH040504-3-LVRU6MP
Lentiviral mouse Lgr4 shRNA2	GeneCopoeia	MSH040504-4-LVRU6MP
Lentiviral scrambled control for shRNAs	GeneCopoeia	CSHCTR001-LVRU6MP
Lentiviral scrambled control for shRNAs	Sigma-Aldrich	SHC216
Lentiviral human LGR4 shRNA 1	Sigma-Aldrich	TRCN0000273532
Lentiviral human LGR4 shRNA 2	Sigma-Aldrich	TRCN0000285015
Lentiviral human GNAS shRNA 1	Sigma-Aldrich	TRCN0000310794
Lentiviral human GNAS shRNA 2	Sigma-Aldrich	TRCN0000303965
Lentiviral human CREB shRNA 1	Sigma-Aldrich	TRCN0000226466
Lentiviral human CREB shRNA 2	Sigma-Aldrich	TRCN0000226467
Lentiviral human CREB shRNA 3	Sigma-Aldrich	TRCN0000226468
Lentiviral human LGR4 gRNA - CRISPR/Cas9	Sigma-Aldrich	HS0000422096
Lentiviral non-targeting control - CRISPR/Cas9	Sigma-Aldrich	CRISPR12

Table S4, related to STAR Methods. qPCR primers used in this study.

Human

Gene	Forward primer sequence (5' → 3')	Reverse primer sequence (5' → 3')
<i>GAPDH</i>	CGCTCTCTGCTCCTCCTGTT	GTTGACTCCGACCTTCC
<i>LGR4</i>	CGGGCAACGACCTTTCTTTTATCC	GGCTTCACTGGGTACTGTTTTCAACT
<i>HOXA9</i>	AAAAACAACCCAGCGAAGGC	GGGTTATTGGGATCGATGGGG
<i>c-FOS</i>	CCAAGCGGAGACAGACCAAC	ATCAGGGATCTTGCAGGCAG
<i>TCF7L2</i>	GACAAGCCCTCAAGGATGCC	CGTCGGCTGGTAAGTGTGG
<i>CCND1</i>	GCCGTCCATGCGGAAGATC	CCTCCTCCTCGCACTTCTGT
<i>MEF2C</i>	CTCAGTCAGTTGGGAGCTTGC	GCGTGTGTTGTGGGTATCTCG
<i>HOXA7</i>	CCCTGGATGCGGTCTTCAG	CAGCTCCAGCGTCTGGTAG
<i>HOXA11</i>	GGCCACACTGAGGACAAGG	AGAACTCCCGTTCCAGCTCT
<i>MEIS1</i>	AGACCAGTCCAACCGAGCAG	CATGGGCTGTCCATCAGGA
<i>GNAS</i>	GCAGACAGATGCGCAAAGAAGC	GCTTTTACCAGATTCTCCAGCAC

Mouse

Gene	Forward primer sequence (5' → 3')	Reverse primer sequence (5' → 3')
<i>Gapdh</i>	CATGGCCTTCCGTGTTCCCTA	CCTGCTTCACCACCTTCTTGAT
<i>c-Fos</i>	GGGCTCTCCTGTCAACACAC	AGTTGGCACTAGAGACGGACA
<i>Tcf7l2</i>	TTCCTCCGATCACAGACCTGAG	GCTGCCTTCACCTTGTATGTAGC
<i>Ccnd1</i>	CAACAACCTTCTCTCCTGCTACC	AGACCAGCCTCTTCTCCAC
<i>Mef2c</i>	GGCTCTGTAACCTGGCTGGCA	GGGTGGTGGTACGGTCTCTA

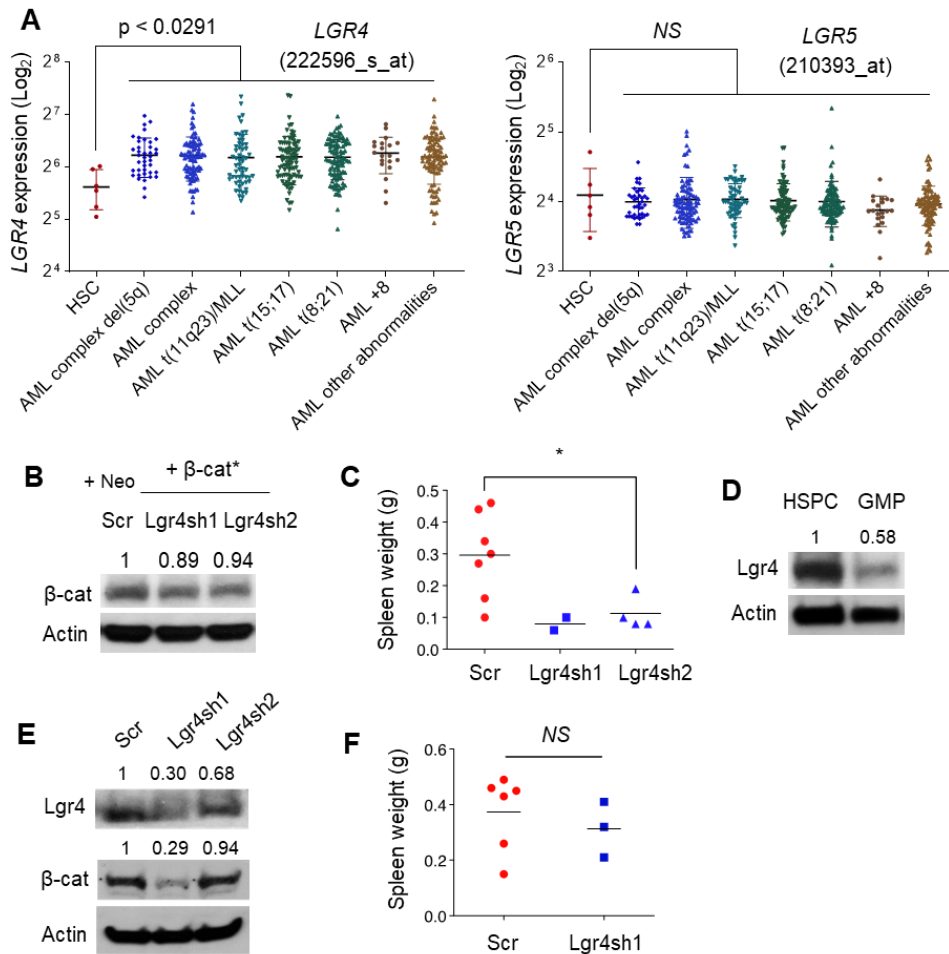


Figure S1, related to Figure 1.

(A) Integrated analysis of 5 independent gene expression datasets (GSE13159, GSE15434, GSE61804, GSE14468, and The Cancer Genome Atlas TCGA) (Bagger et al., 2016) showing upregulation of *LGR4* but no noticeable change of its family member *LGR5* in primary AML patient samples ($n=481$), compared with normal human HSCs ($Lin^-CD34^+CD38^-CD90^+CD45RA^-$; GSE42519). Scatter dot plots represent the mean \pm SD. One-way ANOVA.

(B) Western blots indicating comparable levels between exogenously expressed β -cat* in MLL- AF9-HSPC pre-LSCs carrying Lgr4 shRNAs and endogenous β -catenin in MLL-AF9-HSPC pre-LSCs carrying control vectors (Scr and neo).

(C) Spleen weights of mice with MLL-AF9-HSPC primary AML carrying Scr versus Lgr4 shRNAs. Scatter dot plots represent the mean \pm SD. Unpaired t test. * $p < 0.05$.

(D) Western blots showing relatively higher levels of endogenous Lgr4 expression in HSPC-derived MLL-AF9 pre-LSCs than in GMP-derived MLL-AF9 pre-LSCs.

(E) Western blots showing Lgr4 knockdown and a resultant reduction of endogenous β -catenin protein in Lgr4 shRNA-expressing MLL-AF9-GMP pre-LSCs compared with Scr.

(F) Spleen weights of mice with MLL-AF9-GMP primary AML carrying Scr versus Lgr4sh1. Scatter dot plots represent the mean \pm SD. Unpaired t test. NS, not significant ($p > 0.05$).

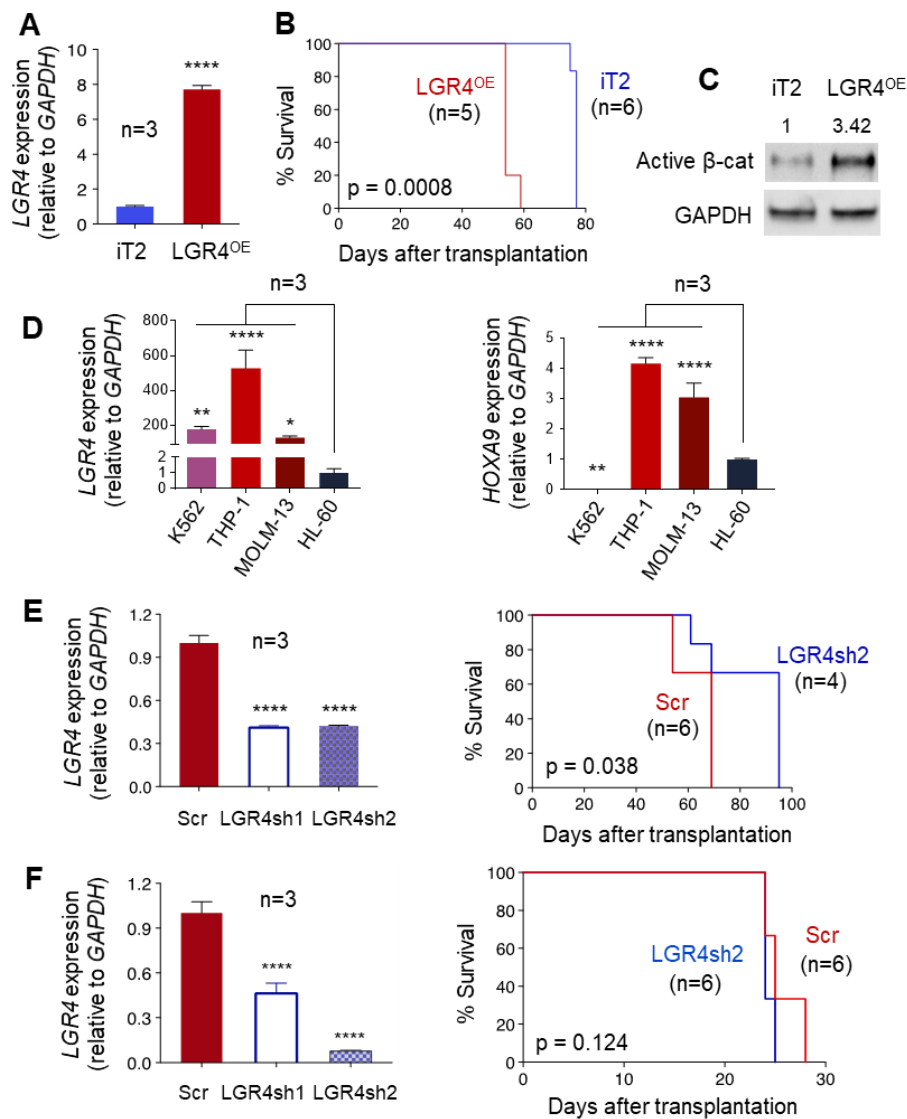


Figure S2, related to Figure 2.

(A) qPCR confirming overexpression of human *LGR4* (*LGR4*^{OE}) in human AML THP-1 cells transduced with LeGO-iT2-*LGR4*. Mean ± SD. n=3 replicates per condition. Unpaired t test. **** p < 0.0001.

(B) Kaplan-Meier survival curves of NSG mice transplanted with 1×10⁶ human THP-1 cells expressing iT2 (n=6 mice) versus *LGR4*^{OE} (n=5 mice) for AML development. P value was determined by the log-rank test.

(C) Western blots confirming *LGR4*^{OE}-induced increase in non-phospho (active) β-catenin in hCD33⁺ myeloid cells isolated from the BM of human AML THP-1 xenografts.

(D) qPCR showing relative mRNA levels of *LGR4* and *HOXA9* in four human myeloid leukemia cell lines. Mean ± SD. n=3 replicates per cell line. * p < 0.05, ** p < 0.005, **** p < 0.0001. One-way ANOVA.

(E) qPCR confirming knockdown levels of *LGR4* in human THP-1 cells carrying Scr versus *LGR4* shRNAs. Mean ± SD. n=3 replicates per condition. **** p < 0.0001. One-way ANOVA. Kaplan-Meier survival curves of NSG mice transplanted with 1×10⁶ THP-1 leukemic cells carrying Scr (n=6 mice) versus *LGR4*sh2 (n=4 mice). P value was determined by the log-rank test.

(F) qPCR confirming knockdown levels of *LGR4* in human K562 cells carrying Scr versus *LGR4* shRNAs. Mean ± SD. n=3 replicates per condition. **** p < 0.0001. One-way ANOVA. Kaplan-Meier survival curves of NSG mice transplanted with 2×10⁶ K562 leukemic cells carrying Scr (n=6 mice) versus *LGR4*sh2 (n=6 mice). P value was determined by the log-rank test.

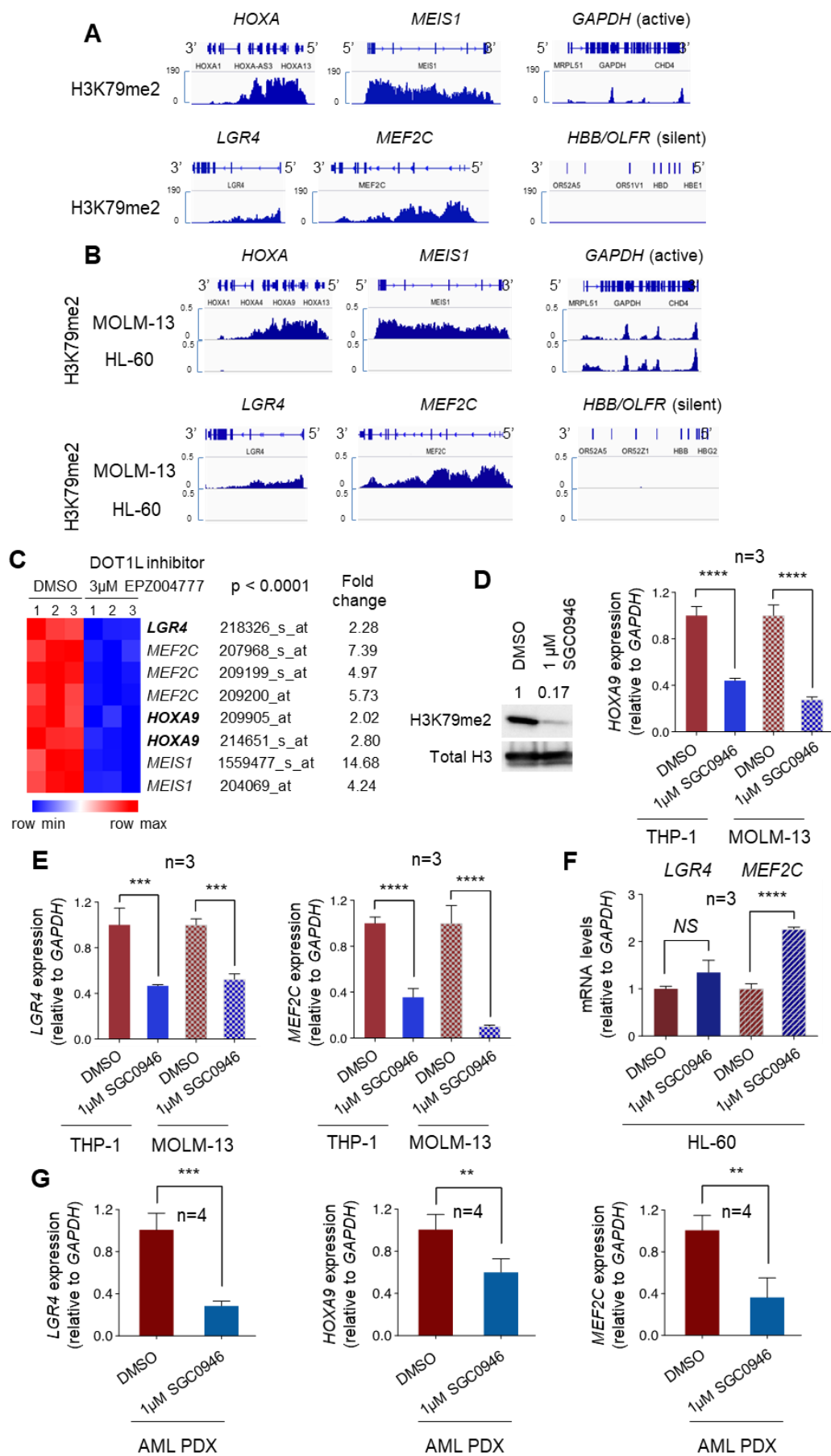


Figure S3, related to Figure 2.

(A and B) IGV visualization of (A) H3K79me2 ChIP-seq (GSM1519628) in human MLL-AF9 AML MOLM-13 cells (Chen et al., 2015), and (B) H3K79me2 ChIP-seq (GSE43063) in MOLM-13 cells and human AML HL-60 cells (Deshpande et al., 2013).

(C) Heat map of gene expression data (n=3, $p < 0.0001$; GSE29828) (Daigle et al., 2011) showing reduced expression of *LGR4*, *MEF2C*, *HOXA9* and *MEIS1* following treatment with 3 μ M EPZ004777 (DOT1L inhibitor) in MOLM-13 cells.

(D) Western blots confirming SGC0946 (DOT1L inhibitor)-induced suppression of H3K79me2 and qPCR confirming SGC0946-induced reduction in *HOXA9* expression in human MLL-AF9 AML MOLM-13 and THP-1 cells. n=3 replicates per condition.

(E) qPCR showing SGC0946-induced repression of *LGR4* and *MEF2C* expression in MOLM-13 and THP-1 cells. n=3 replicates per condition.

(F) qPCR revealing no inhibitory effects of 1 μ M SGC0946 on expression of *LGR4* and *MEF2C* in human HL-60 cells. n=3 replicates per condition.

(G) qPCR showing SGC0946-induced decrease in expression of *LGR4*, *HOXA9* and *MEF2C* in human CD33⁺ AML PDX cells. n=4 replicates per condition.

Data are represented as the mean \pm SD. Unpaired t test. ** $p < 0.005$, *** $p < 0.0005$, **** $p < 0.0001$; NS, not significant ($p > 0.05$).

Table S1, related to Figures 3 and S4.

DNMT3A	NM_175629	Exon 23: c.2644C>A:p.R882S	nonsynonymous SNV
RUNX1	NM_001754	Exon 5: c.408T>G:p.N136K	nonsynonymous SNV
KRAS	NM_004985	Exon 2:c.35G>C:p.G12A	nonsynonymous SNV
NRAS	NM_002524	Exon 3:c.181C>A:p.Q61K	nonsynonymous SNV
PTPN11	NM_002834	Exon 3: c.181G>C:p.D61H	nonsynonymous SNV
ETV6	NM_001987	Exon 5: c.641C>T:p.P214L	nonsynonymous SNV
BCOR	NM_017745	Exon 4: c.2048_2049C	frameshift substitution

Mutational profiles of primary PDX cells (relapsed AML) identified by targeted next-generation deep sequencing (NGS). *Note:* A nonsynonymous SNV (single nucleotide variation) is a single nucleotide mutation that alters an amino acid in the corresponding codon.

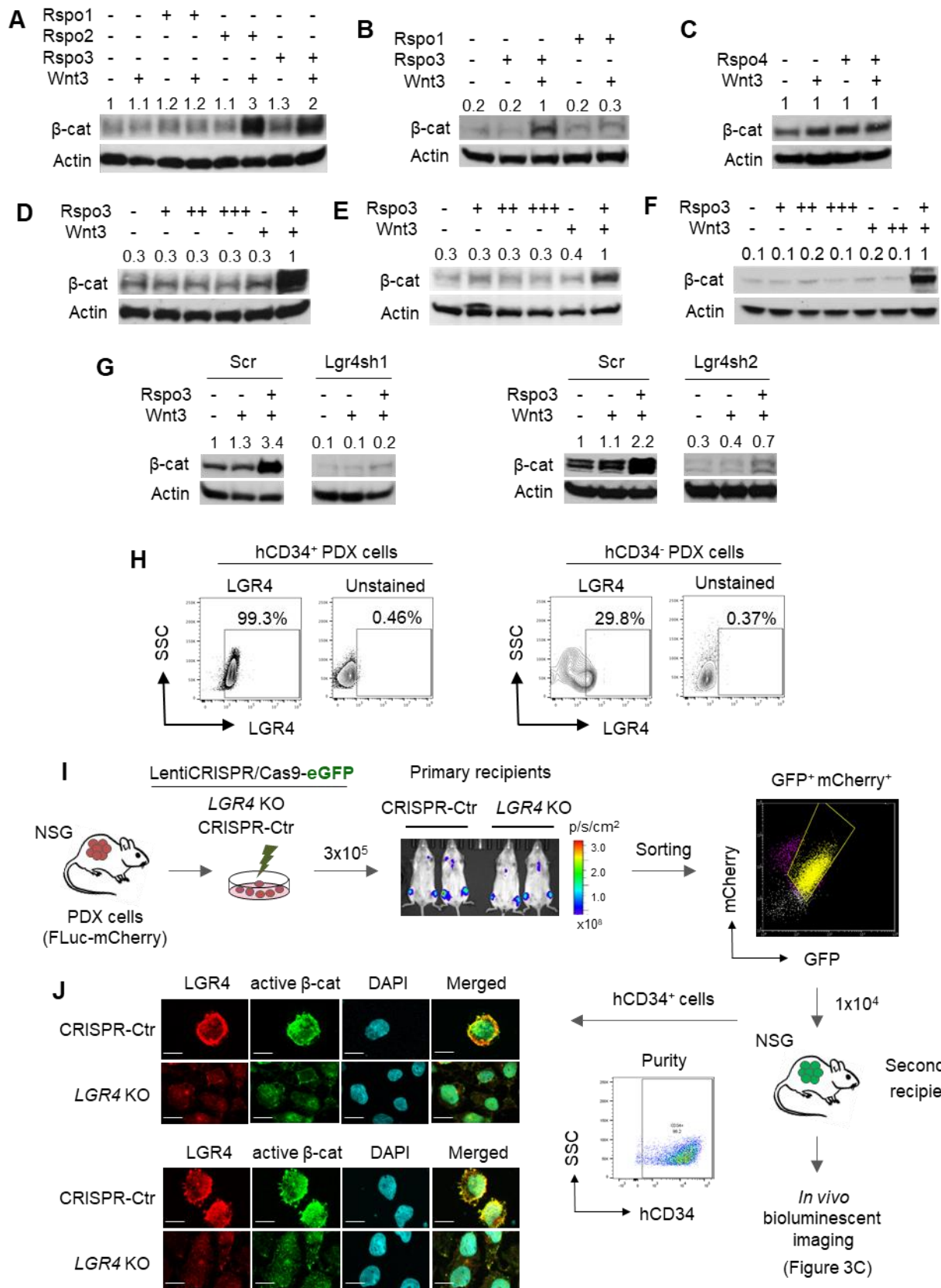


Figure S4, related to Figure 3 and Table S1.

(A-F) Western blots showing changes in endogenous expression of β -catenin in MLL-AF9- HSPC pre-LSCs (A-D), MLL-AF9-GMP pre-LSCs (E) and HOXA9/MEIS1 (A9M)-HSPC pre-LSCs (F), following 24 h of culture with indicated concentrations of Rspo, Wnt3 or their combination. Rspo: +, 50 ng/mL; ++, 100 ng/mL; +++, 200 ng/mL and Wnt3 (L-Wnt3): +, 1 in 10 v/v; ++, 1 in 5 v/v.

(G) Western blots showing that Lgr4 depletion blocked Rspo3/Wnt3-mediated β -catenin activation in MLL-AF9-HSPC pre-LSCs, following 24 h of culture with Wnt3 or a combination of Rspo3 and Wnt3.

(H) Flow cytometry plots showing the percentage of LGR4-expressing cells in hCD34⁺ versus hCD34⁻ subpopulations of primary AML PDX cells.

(I) Schematic outline of the experimental procedure for generation of lentiCRISPR-Cas9-mediated knockout (KO) of *LGR4* in primary AML PDX model. Briefly, FLuc-mCherry-expressing human PDX AML cells were stably transduced for 4 h with non-targeting-Cas9-eGFP control (CRISPR-Ctr)-expressing versus LGR4-Cas9-eGFP (*LGR4* KO)-expressing lentiviral particles in RPMI-1640 medium supplemented with 8 μ g/mL polybrene, 20% FCS, 5% L-Glutamin, 0.6% mixture of recombinant human insulin/human transferrin/sodium selenite (Life technologies), 1 mM sodium pyruvate, 100 ng/mL SCF, 100 ng/mL Flt3-ligand (Flt3-L), 60 ng/mL IL-3 and 10 ng/mL TPO. 3×10^5 transduced cells were transplanted into NSG mice and after 63-day expansion in NSG mice, GFP⁺mCherry⁺ CRISPR-expressing PDX cells collected from mouse BM were transplanted into secondary recipient mice for monitoring leukemia burden using *in vivo* bioluminescence imaging (see Figure 3E).

(J) Representative IF images showing changes in membrane protein LGR4 and nuclear active non-phospho- β -catenin in hCD34⁺ cells isolated from CRISPR-Ctr and *LGR4* KO PDX mice of primary human AML. Two technical replicates are shown. FACS analysis shows representative purity of hCD34⁺ population obtained using this protocol. Scale bar, 10 μ m.

Table S2, related to Figures 4 and S5.

AML Diagnosis	<i>LGR4</i> Expression	<i>HOXA9</i> Expression	Response to RSPO2/RSPO3
9p deletion	+	+	+
MLL-AF9	+	+	+
MLL-AF1q	+	+	+
MLL-AF10 (relapse)	+	+	+
MLL-AF10	+	+	+
AML1-ETO	+	-	+/-
Normal karyotype	+	-	+/-

Correlation between LGR4/HOXA9 expression and the RSPO response in primary AML patient samples. -, no/little expression; +/-, little response; +, expression and response to RSPO stimulation.

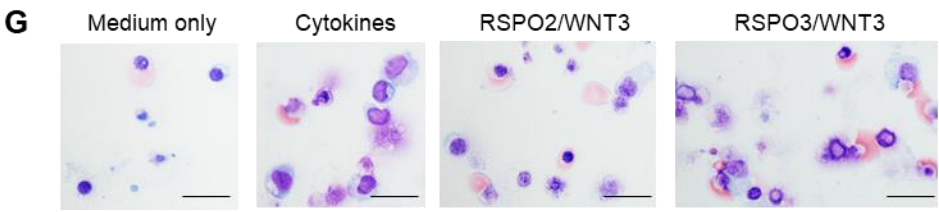
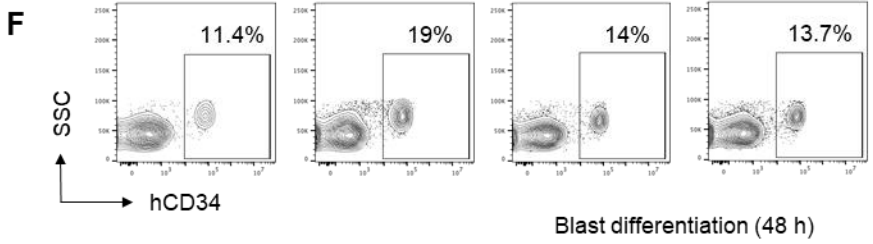
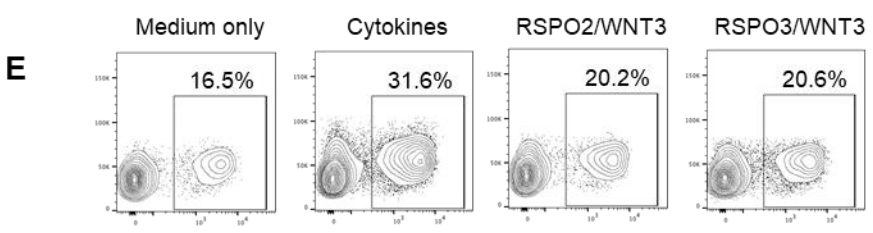
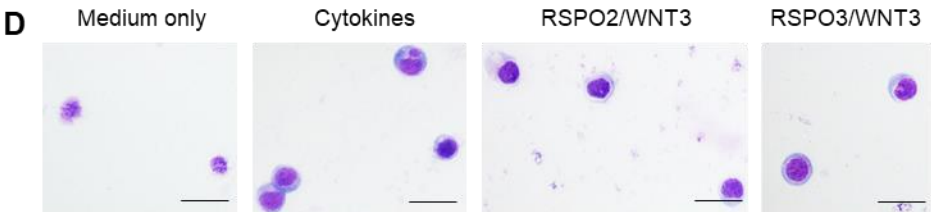
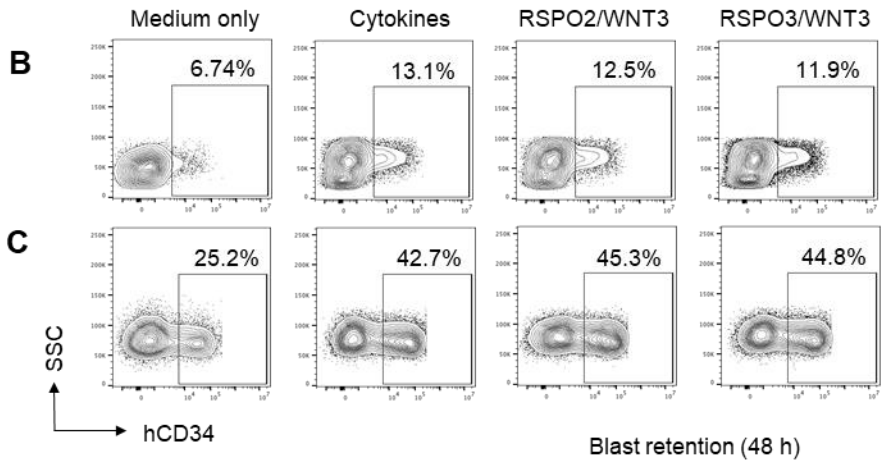
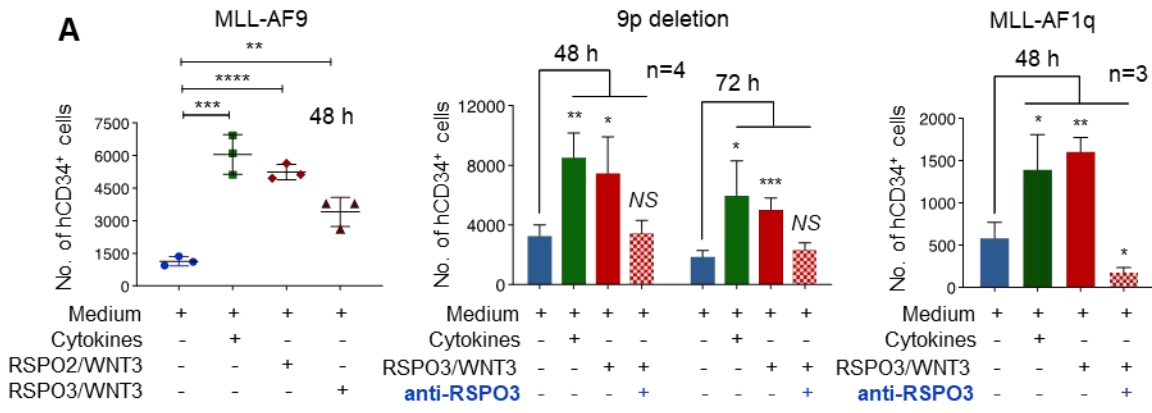


Figure S5, related to Figure 4 and Table S2.

(A) Absolute numbers of viable hCD34⁺ immature cells in primary AML patient specimens harboring MLL-AF9 (n=3), 9p deletion (n=4) or MLL-AF1q (n=3), after 48 h or 72 h of culture in indicated media conditions. Medium: RPMI 1640 supplemented with 1% FBS; +, 200 ng/mL RSPO2/RSPO3/WNT3 with or without 150 µg/mL anti-RSPO3 antibody in the medium. Mean ± SD. Unpaired t test. * p < 0.05, ** p < 0.005, *** p < 0.0005, **** p < 0.0001; NS, not significant (p > 0.05).

(B and C) Representative flow cytometry plots showing percentages of hCD34⁺ cells present in diagnosis (B) or relapse (C) AML patient specimens harboring MLL-AF10, after 48 h of culture in indicated media conditions.

(D) Wright-Giemsa staining of relapse AML patient blasts with MLL-AF10 (×60 magnification) after 48 h of culture in indicated media conditions. Scale bar, 20 µm.

(E and F) Representative flow cytometry plots showing percentages of hCD34⁺ cells present in primary AML patient specimens harboring AML1-ETO (E) or with normal karyotype (F), after 48 h of culture in indicated media conditions.

(G) Wright-Giemsa staining of primary AML patient blasts with normal karyotype (×60 magnification) after 48 h of culture in indicated media conditions. Scale bar, 20 µm.

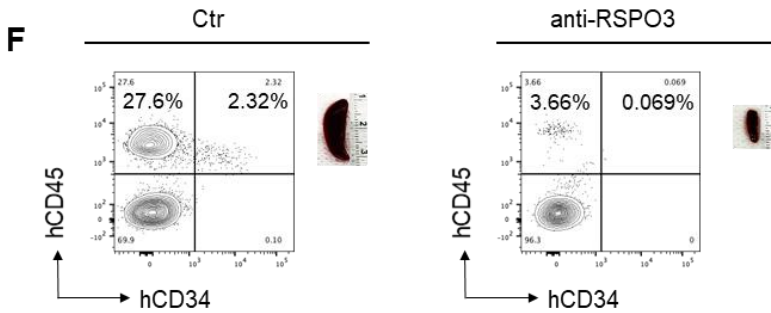
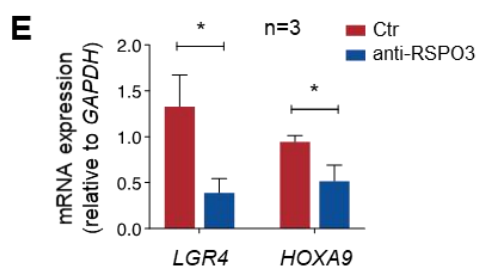
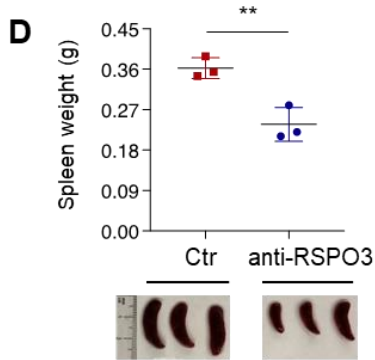
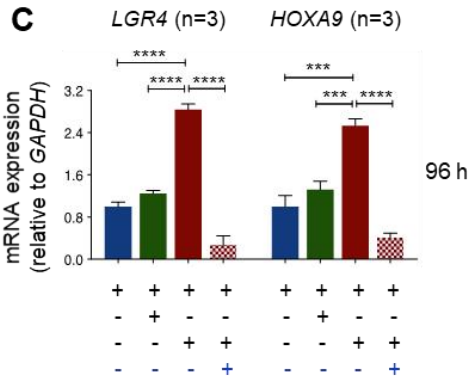
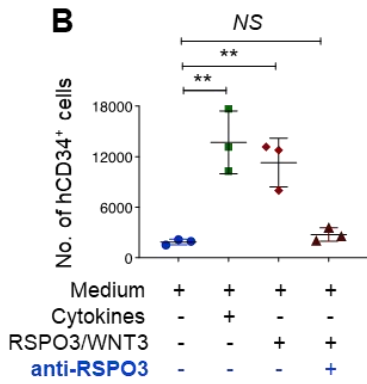
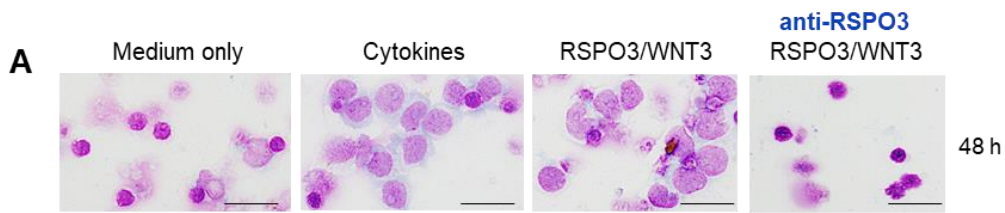


Figure S6, related to Figure 4.

(A) Wright-Giemsa staining ($\times 60$ magnification) of primary AML PDX cells, after 48 h of culture in indicated media conditions. Scale bar, 20 μm .

(B) Absolute numbers of viable hCD34⁺ immature cells from primary AML PDX cells after 96 h of culture in indicated media conditions. n=3 replicates.

(C) qPCR showing relative mRNA levels of *LGR4* and *HOXA9* in primary AML PDX cells after 96 h of culture in indicated media conditions. n=3 replicates per condition.

(D) Spleen weights of NSG mice engrafted with primary AML patient specimen harboring 9p deletion followed by *in vivo* anti-RSPO3 treatment (20 mg/kg, i.p. every 4 days). Spleens were collected 154 days after transplantation and images showing spleen sizes of these NSG mice.

(E) qPCR displaying relative mRNA levels of *LGR4* and *HOXA9* in the BM of NSG mice engrafted with primary AML patient specimen harboring 9p deletion, followed by *in vivo* anti-RSPO3 treatment. n=3 replicates per condition. Data are representative of at least 3 independent repeats

(F) Flow cytometry plots depicting the percentage of hCD34⁺ hCD45⁺ leukemic cells in the spleen of NSG mice engrafted with primary AML patient specimen harboring MLL-AF9, followed by *in vivo* anti-RSPO3 treatment (20 mg/kg, i.p. every 4 days). Spleens were collected and harvested 83 days after transplantation and images showing spleen sizes of these NSG mice.

Mean \pm SD. Unpaired t test. * $p < 0.05$, ** $p < 0.005$, *** $p < 0.0005$, **** $p < 0.0001$; NS, not significant ($p > 0.05$).

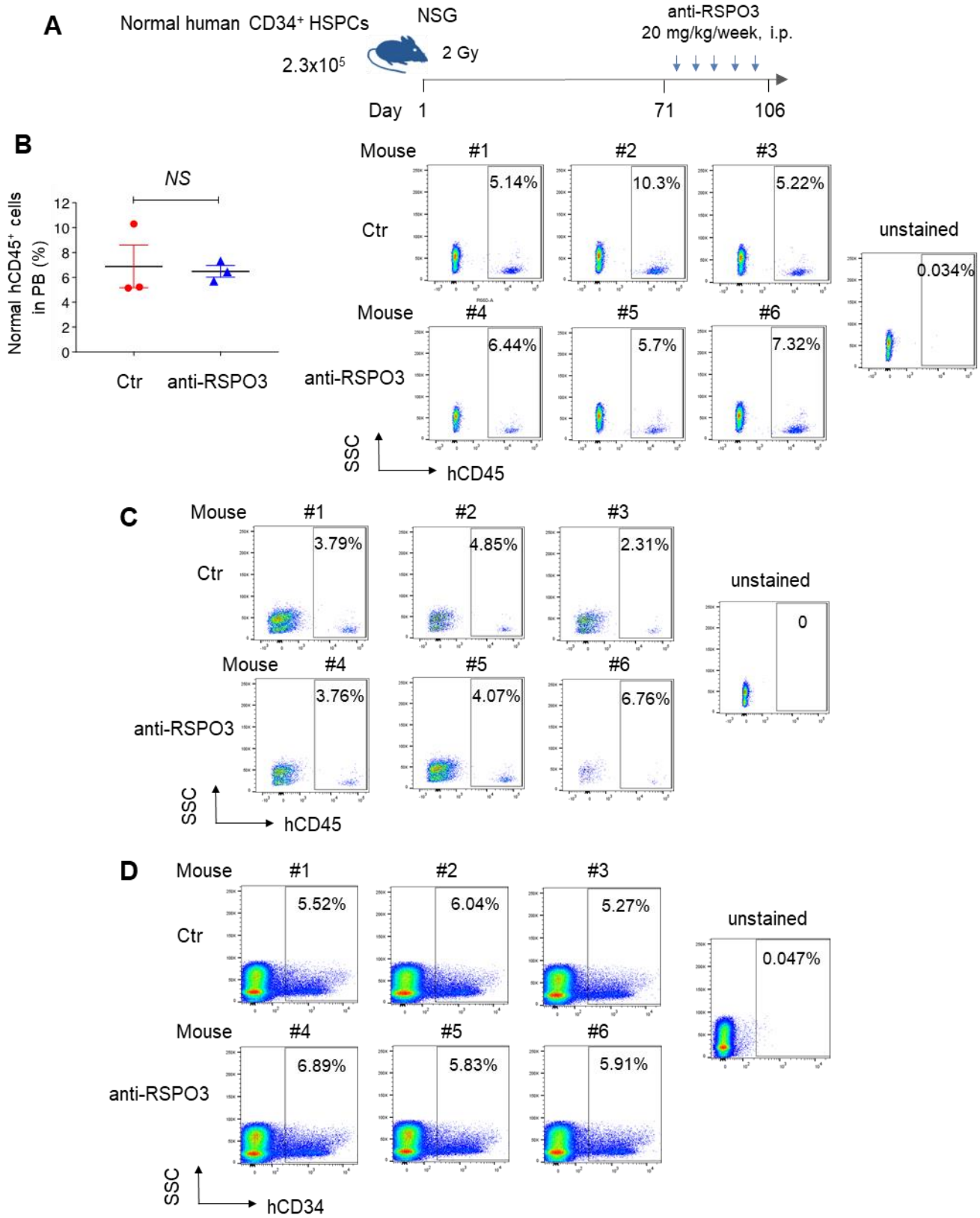


Figure S7, related to Figure 5.

(A) Schematic outline of the experimental procedure. 2.3×10^5 normal human CD34⁺ HSPCs from the BM of healthy donors were transplanted into sublethally irradiated (2 Gy) NSG recipient mice.

(B) Dot plots and flow cytometry plots depicting percentages of normal hCD45⁺ cells engrafted in the peripheral blood (PB) of NSG recipient mice 71 days after transplantation (before *in vivo* treatment). Six engrafted mice were randomly allocated to two groups for subsequent *in vivo* anti-RSPO3 treatment. Mean \pm SD. n=3 mice per group. Unpaired t test. *NS*, not significant ($p > 0.05$).

(C) Flow cytometry plots depicting percentages of normal hCD45⁺ cells engrafted in the PB of NSG recipient mice 106 days after transplantation, following *in vivo* anti-RSPO3 treatment (20 mg/kg body weight, i.p. once per week for 5 weeks).

(D) Flow cytometry plots depicting percentages of normal hCD34⁺ HSPCs engrafted in the BM of NSG recipient mice 106 days after transplantation, following *in vivo* anti-RSPO3 treatment (20 mg/kg body weight, i.p. once per week for 5 weeks).

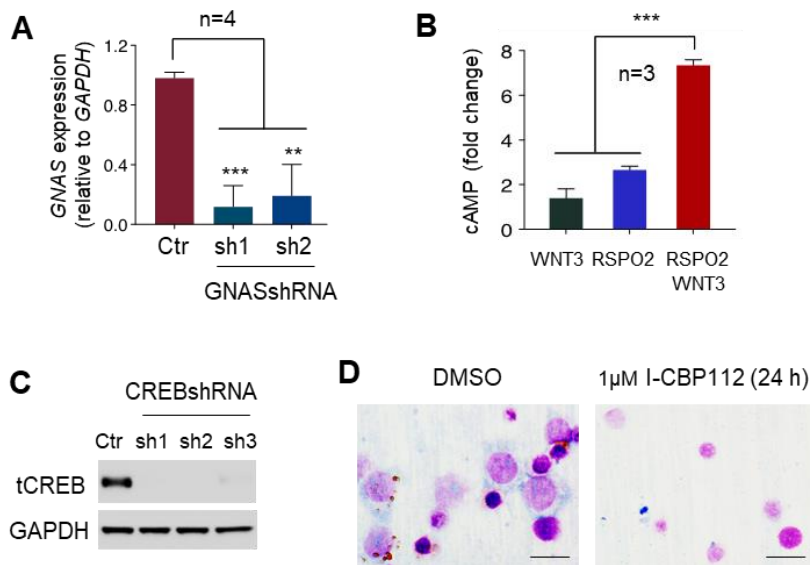


Figure S8, related to Figure 6.

(A) qPCR confirming knockdown levels of *GNAS* in human AML THP-1 cells carrying Scr versus *GNAS* shRNAs. Data are representative of at least 3 independent repeats. Mean \pm SD. n=4 replicates per condition. **** p < 0.0001. One-way ANOVA.

(B) The cAMP-Glo assay showing changes in cAMP concentrations of human AML THP-1 cells, following 5 h of culture with 200 ng/mL of RSP02/WNT3 ligands, alone or in combination. Mean \pm SD. n=3 replicates per condition. *** p < 0.0005. One-way ANOVA.

(C) Western blots confirming sufficient knockdown of CREB by shRNAs in human AML THP-1 cells.

(D) Wright-Giemsa staining ($\times 60$ magnification) of hCD33⁺ AML PDX cells treated with DMSO versus 1 μ M I-CBP112 for 24 h. Scale bar, 10 μ m.